Climate Dynamics (2019) 52:5877–5897
https://doi.org/10.1007/s00382-018-4485-8

Separate tree-ring reconstructions of spring and summer moisture in the northern and southern Great Plains

Ian M. Howard[1] · **David W. Stahle**[1] · **Song Feng**[1]

Received: 29 May 2018 / Accepted: 4 October 2018 / Published online: 11 October 2018

Abstract
The two most severe droughts to impact the Great Plains in the twentieth century, the 1930s Dust Bowl and 1950s Drought, were the result of multiyear moisture deficits during the spring and especially the summer season. Tree-ring reconstructions of the Palmer Drought Severity Index indicate similar droughts in magnitude have occurred in previous centuries, but these reconstructions do not capture the potential distinct seasonal drought characteristics like those of the 1930s and 1950s. Separate tree-ring reconstructions of the spring and summer Z-index based on earlywood, latewood, and adjusted latewood width chronologies have been developed for two regions in the northern and southern Great Plains of the US. The reconstructions extend from 1651 to 1990 and 1698–1990, respectively, with instrumental data added from 1991 to 2017. The four reconstructions explain from 39 to 56% of the variance during the 1945–1990 calibration interval and are significantly correlated with independent moisture balance observations during the 1900–1944 validation period. The reconstructions reproduce similar seasonal sea-surface temperature and 500 mb geopotential height spatial correlation patterns detected with the instrumental data. The 1930s is estimated to have been the most extreme decadal summer drought to impact the two regions concurrently in the last few centuries. On average, spring moisture deficits were more severe during the multidecadal droughts of the mid- to late-nineteenth century, but the timing of drought onset and termination differed between the study regions. In the recent two decades the spring moisture balances for the two study regions have largely been opposite, and this has been one of the most extreme periods of anti-phasing in the last few centuries. Seasonal moisture reversals are not randomly distributed in time based on the reconstructed estimates and are related to sea-surface temperature anomalies in the tropical Pacific and to mid-tropospheric circulation changes over the North Pacific–North American sector during May and June.

1 Introduction

Precipitation during the spring (March–May) and summer (June–August) months is a vital water resource for the North American Great Plains. The spring and summer seasons account for 70% of the total annual precipitation, with 30% occurring in spring, and 40% in summer (Mock 1996; Wang and Chen 2009). Springtime precipitation can result from several different atmospheric circulation features, most prominently mid-latitude storm systems, frontal boundaries, and leeside cyclogenesis in the central and eastern Rocky Mountains (Mock 1996). During summer, deep convection, and less commonly, synoptic-scale disturbances produce a significant portion of summer rainfall (Dai 2001). The Great Plains low-level jet (GPLLJ) is an important component to both spring and summer moisture (Higgins et al. 1997). Major synoptic weather systems in spring can increase the advection of low-level moisture from the Gulf of Mexico, creating atmospheric environments that promote widespread precipitation over the Great Plains (Hirschboeck 1991). Though less frequent than spring, shortwave disturbances and major frontal systems passing over the Great Plains can deliver significant amounts of moisture in summer. But deep convection is more common during the summer months when the GPLJJ reaches its maximum strength and southerly low-level moisture advection is highest over the Great Plains (Weaver and Nigam 2008). Strong southerly moisture advection can generate convective precipitation at local to regional scales even in the absence of major synoptic forcing

Electronic supplementary material The online version of this article (https://doi.org/10.1007/s00382-018-4485-8) contains supplementary material, which is available to authorized users.

✉ Ian M. Howard
ihowardksu@gmail.com

[1] Department of Geosciences, University of Arkansas, Fayetteville, AR, USA

(Weaver and Nigam 2011). Convective activity that forms along areas of low-level moisture convergence sometimes evolves into major mesoscale convective systems that move eastward across the plains during the evening and nighttime hours, providing one of the most important sources of summertime precipitation to the region (Fritsch et al. 1986; Higgins et al. 1997).

The atmospheric and sea-surface temperature (SSTs) teleconnection patterns vary both regionally and seasonally across the Great Plains. The El Niño Southern Oscillation (ENSO) significantly influences precipitation and temperature over the southern and central Great Plains in the winter and spring seasons by causing perturbations in mean atmospheric circulation (Ropelewski and Halpert 1987). The tropical Pacific SST teleconnection weakens into summer, but studies have shown that positive phases of spring–summer ENSO can lead to above normal summer precipitation in the northern Great Plains (Bunkers et al. 1996). Other major ocean-atmospheric modes of variability that influence both spring and summer moisture include the Arctic Oscillation (Hu and Feng 2010); the North Atlantic Oscillation (NAO; Ruiz-Barradas and Nigam 2005), and the Pacific-North American pattern (Leathers et al. 1992). These sources of seasonal forcing primarily alter the latitudinal position and strength of the upper-level westerly jet stream (as with the PNA in spring; Leathers et al. 1992), and the advection of low-level moisture from the Gulf of Mexico (as with the AO and NAO in summer; Weaver and Nigam 2008; Hu and Feng 2010). At longer timescales (e.g. decadal to multidecadal), spring and summer moisture variability are influenced by low frequency SST fluctuations in both the Atlantic and Pacific, manifested in the Atlantic Multidecadal Oscillation (AMO; Enfield et al. 2001) and the Pacific Decadal Oscillation (PDO; Mantua and Hare 2002). The seasonal impacts of these slowly varying modes of SST variability are realized in their decadal-to-multidecadal effects on other teleconnections (e.g. ENSO) and large-scale atmospheric circulation.

The Great Plains has been impacted by a number of sustained multiyear drought episodes in both the instrumental and historical period (Woodhouse and Overpeck 1998). Drought in the Great Plains, and the associated agricultural, ecological, and socioeconomic impacts are primarily the result of severe moisture deficits that accrue during the spring and summer since these are the seasons when the bulk of the precipitation occurs (Karl et al. 1987). The two most severe and sustained droughts to impact the Great Plains in the instrumental period, the 1930s Dust Bowl and 1950s Drought, were the result of multiyear moisture deficits during the spring, but especially the summer season over the regions most impacted by drought conditions. During the 1930s over the central and Northern Great Plains, and in the 1950s over the Southern Great Plains, only modest precipitation deficits were present (Fig. 1a, b). But during summer,

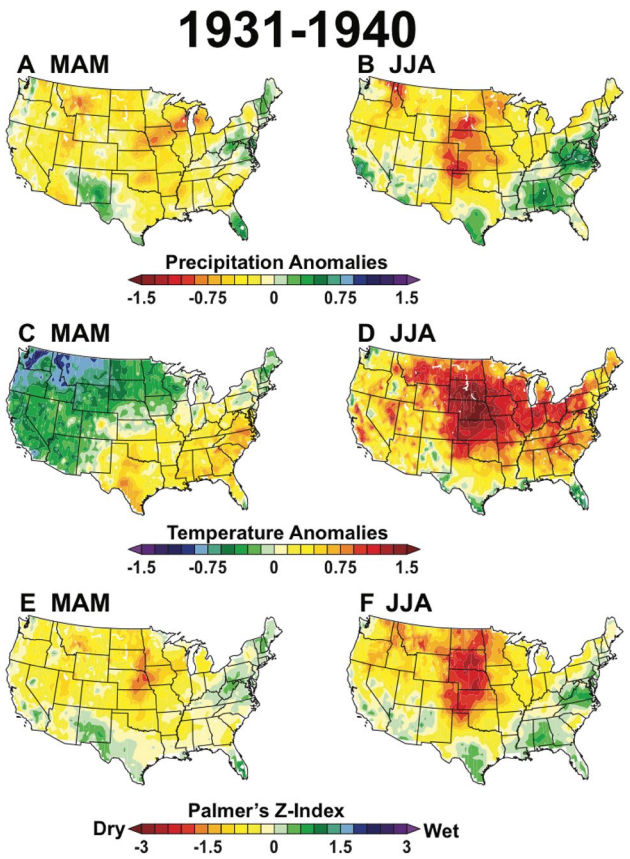

Fig. 1 **a, b** Normalized precipitation for the **a** spring (MAM) and **b** summer (JJA) seasons are plotted for the Dust Bowl period using the gridded PRISM dataset. **c, d** Same as **a, b** but with temperature data. **e, f** Same as **a, b** but with Palmer's Z-index. Note that in all cases, conditions intensified and expanded from spring to summer

the precipitation anomalies were much more widespread and severe (Figs. 1b, 2b). Temperature anomalies were also more extreme in summer, and these conditions acted to exacerbate drought conditions during extreme summer droughts like in 1934 and 1936 (Figs. 1c, d, 2c, d; Donat et al. 2016). The intensification of drought from spring to summer during the 1930s and 1950s is also well represented by the instrumental Palmer's Z-index (Figs. 1e, f, 2e, f; Palmer 1965); the atmospheric moisture balance calculated from precipitation and temperature measurements but without the strong monthly persistence prescribed for the soil moisture formulation of the full Palmer Drought Severity Index (PDSI). A number of the most intense single-year summer droughts outside of the 1930s and 1950s (e.g. 1988 and 2011) also exhibited a similar intensification of dry conditions from spring to summer, potentially arising through land–surface interactions that cause persistence in atmospheric circulation anomalies across seasons (Hoerling et al. 2013).

However, spring climate conditions are typically not a reliable predictor of summer precipitation totals over the

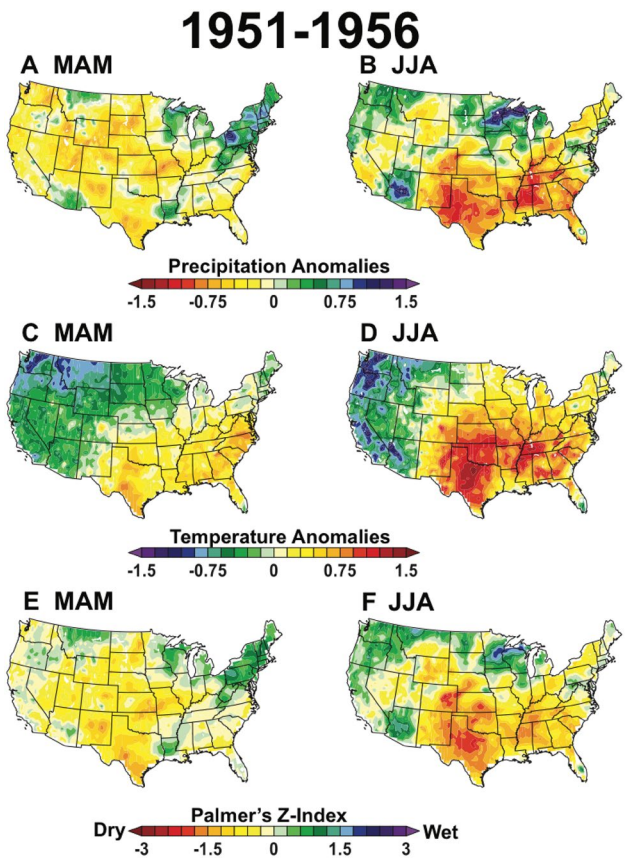

Fig. 2 Same as Fig. 1, but for the 1950s Drought from 1951 to 1956. Similar to the Dust Bowl Drought, the largest anomalies took place during the summer season, but drought conditions were more centered over the Southern Plains and Southeast

Great Plains, and there have been numerous years of opposing seasonal moisture anomalies in the instrumental record. These seasonal "moisture reversals", defined as below-normal spring precipitation preceding a wet summer and vice versa, are largely unpredictable on seasonal timescales (Hoerling et al. 2014) and pose numerous challenges to agricultural and water resource planning. Examples of seasonal moisture reversals include the "flash droughts" of 1980 and 2012, when near-to-above normal spring moisture and average temperatures rapidly transitioned into severe drought conditions in the late-spring and early-summer over the central and southern US (Karl et al. 1981; Mo and Lettenmaier 2016). Developing proxy records that can separately model spring and summer moisture variability could allow for the examination of the multi-century history of the two most important seasons to the precipitation climatology of the Great Plains, and possibly provide a longer baseline for the frequency of drought intensification events and major moisture reversals. In the Great Plains, it may be possible to reconstruct seasonal climate variability using sub-annual tree-ring proxies from the region.

Investigation of climate variability at interannual, decadal, and multidecadal timescales can be augmented with historical and paleoclimate data (Muhs and Holliday 1995; Meko and Baisan 2001; Mock 1991; Stahle et al. 2009; Burnette and Stahle 2013; Griffin et al. 2013). Moisture sensitive tree-ring data have provided high-resolution estimates for past droughts and pluvials at local to continental scales, including in the Great Plains. Tree-ring chronologies from the Great Plains have been used to reconstruct variables that tend to integrate climate conditions across several seasons, such as annual precipitation totals (e.g. Cleaveland and Duvick 1992; Sauchyn and Skinner 2001) or more commonly the PDSI (e.g. Stockton and Meko 1983; Stahle and Cleaveland 1988; Cook et al. 1999, 2007; Woodhouse and Brown 2001, St. George et al. 2009). The annual precipitation and soil moisture signals are strong in many tree-ring chronologies of total-ring width (TRW) from the Great Plains. But the integrative nature of these variables potentially masks important seasonal climate information in the pre-instrumental record.

It is possible to separately estimate seasonal climate conditions from tree rings by using intra-annual earlywood (EW) and latewood (LW) width chronologies. Many North American tree species exhibit a distinct transition between EW (or springwood) and LW (or summerwood) portions of the annual ring, and the year-to-year growth variability in these intra-annual growth characteristics may contain useful proxy information on climate at seasonal timescales (Schulman 1942). For instance, cool season precipitation totals in Mexico and the southwestern US have been reconstructed from EW width chronologies of Douglas-fir and ponderosa pine (Cleaveland et al. 2003; Villanueva-Diaz et al. 2007; Stahle et al. 2009). Latewood and the so-called adjusted latewood (LWa) chronologies from these regions tend to be correlated with summer moisture and have been used to reconstruct precipitation totals associated with the North American Monsoon (Meko and Baisan 2001; Therrell et al. 2002; Stahle et al. 2009; Faulstich et al. 2013; Griffin et al. 2013; Woodhouse et al. 2013). Torbenson and Stahle (2018) recently produced two separate reconstructions of May self-calibrating PDSI and the summer Z-index for the south-central US from TRW, EW, and LW chronologies to examine the interannual to multidecadal relationship between cool season soil moisture and the summer moisture balance. Earlywood and LW chronologies have also been used to estimate more integrative moisture variables like PDSI in east-central Mexico (Burns et al. 2014) and annual precipitation totals in the southern Canadian Cordillera (Watson and Luckman 2004). Several studies have also investigated the seasonal climate response of EW and LW chronologies from Douglas-fir and ponderosa pine sites in the Pacific Northwest and interior Rocky Mountains (Watson and Luckman 2002; Crawford et al. 2015; Dannenberg and Wise 2016).

Earlywood and LW width chronologies have yet to be developed for the Great Plains, therefore the potential for seasonal moisture reconstructions has yet to be examined.

In this paper, we develop separate spring and summer reconstructions of Palmer's Z-index based on a new network of EW, LW, and LWa chronologies for two sub-regions located in the western Great Plains of the US. The Northern Plains study area includes western North and South Dakota, eastern Montana, and eastern Wyoming, along with EW and LW width chronologies from the vicinity. The Southern Plains study region encompasses areas of southeastern Colorado, western Kansas, northeastern New Mexico, and the panhandles of Oklahoma and Texas, with EW and LW width chronologies developed from escarpment woodlands in this region. The Z-index reconstructions are used to examine the history of both spring and summer moisture variability in the northern and southern Plains study areas for the past 300 + years, to investigate the persistence and reversals of moisture conditions from spring to summer, and to explore the possible influence of large-scale ocean-atmospheric variability on changes in spring to summer moisture.

2 Data and methods

2.1 Instrumental climate data

We used Palmer's (1965) original formulation of the Z-index to represent the 'discrete' non-overlapping spring and summer moisture balance. The PDSI is first calculated by computing monthly soil moisture departures based on the supply and demand of water at the surface along with local climate conditions (Palmer 1965; Karl 1986; Feng et al. 2017). These monthly values, called the Z-index (or the monthly moisture anomaly index), represent short-term moisture fluctuations sensitive to deficiencies and excesses on monthly timescales. Unlike the PDSI, the Z-index does not have the statistical autocorrelation coefficient built into its calculation. The Z-index (Palmer 1965) was chosen to represent spring and summer climate variability because drought is often a combination of precipitation and temperature departures, both of which can impact tree growth (Fritts 1965). The Z-index was calculated from gridded precipitation and temperature data obtained from the 4 km resolution Parameter-elevation Regression on Independent Slopes Model (PRISM) dataset for the period 1895–2015 (Daly et al. 1994) and then re-gridded to 0.5° resolution.

Monthly precipitation, temperature, and Z-index data were averaged into the spring (March–May) and summer (June–August) seasons. These seasons were analyzed given their importance to the region's annual rainfall climatology and their high interannual variability (Mock 1996; Seager et al. 2005). We also hypothesized that EW tree growth in this region is best correlated with spring moisture, and LW growth is most responsive to summer rainfall. Gridded monthly SST (Kaplan et al. 1998) and 500 mb geopotential height anomaly data from the twentieth Century Reanalysis Project V2 provided by the NOAA/OAR/ESRL (Compo et al. 2011) were used to identify the large-scale SST and atmospheric circulation influences on the observed and reconstructed seasonal moisture balances for the two regions. We calculated gridded SST and 500 mb height anomalies relative to 1951–1980 climatology.

2.2 EW and LW chronology development

Earlywood and LW width tree-ring chronologies were developed using samples of ponderosa pine (*Pinus ponderosa*) and Douglas-fir (*Pseudotsuga menziesii*) collected from sites located in the western Great Plains. The eastern range of these species in the US extends east of the Rocky Mountains into the western Great Plains, with extensive stands present in the Black Hills of South Dakota and eastern Wyoming, and more isolated populations in eastern Montana and western North Dakota (Wells et al. 1965; Little 1971). Southward in eastern Colorado and New Mexico, ponderosa pine stands typically occupy higher elevation sites on isolated bluffs, escarpments, and mesas (Woodhouse and Brown 2001). Populations of Douglas-fir are rare in the western Great Plains, but a stand located on an isolated bluff in the Black Forest region of east-central Colorado was identified and sampled by Woodhouse and Brown (2001). Previous investigators have sampled many of these western Great Plains' sites and produced chronologies of TRW (e.g. Stockton and Meko 1983; Sieg et al. 1996; Woodhouse and Brown 2001). We obtained the samples from 13 of these sites from the University of Arizona's Laboratory of Tree-Ring Research archives. We made additional collections at one new site (Sierra Grande) and resampled at another (Kenton) in northeastern New Mexico in the spring of 2015. The 15 sites are clustered into two regions of the western Great Plains, a northern network in the Dakota states and Wyoming, and a southern network in eastern Colorado and New Mexico (Fig. 3; Table 1). Each collection is composed of 15–85 increment core specimens and/or cross-sections from living or dead trees, and the annual rings were dated using dendrochronological methods (Stokes and Smiley 1996).

We implemented the techniques outlined by Stahle et al. (2009) to re-measure each sample for EW and LW width. Chronologies were computed using the signal free method of ring-width standardization (Melvin and Briffa 2008; Cook et al. 2014). Signal free detrending preserves high-to-medium frequency variance by iteratively dividing the long-term growth curve into the original measurement data until the common signals inherent in the individual series are maximized. The data were power transformed and detrended

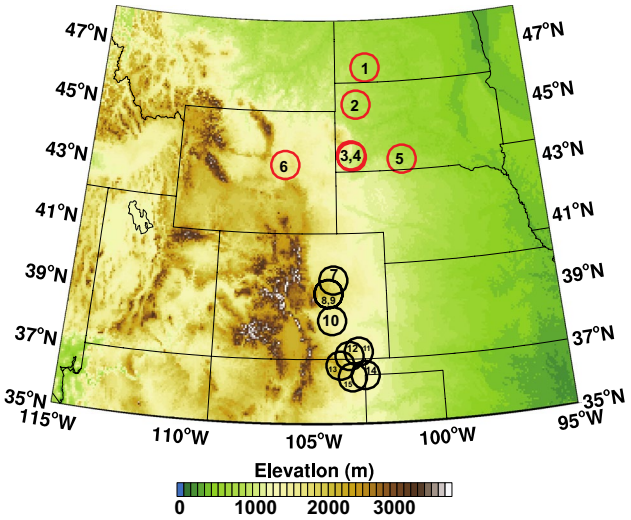

Fig. 3 Locations of the Douglas-fir and ponderosa pine study sites from the western Great Plains used in the analysis. Red circles indicate the northern network (Table 1a) and black circles are part of the southern network (Table 1b). The numbering of each circle corresponds to the sites listed in Table 1

with an age-dependent cubic smoothing spline. Ring-width indices were computed as residuals from the fitted curve, and then averaged into the mean index chronology using the biweight robust mean (Cook 1985; Hoaglin et al. 2000).

Adjusted LW chronologies were also computed using the procedures described by Meko and Baisan (2001). LW growth tends to be highly correlated with the antecedent EW due in large part to biological persistence. Meko and Baisan (2001) used a bivariate regression model to remove this seasonal growth dependency, where the LW predictor chronology was regressed on the EW predictand chronology. The residuals from this regression are the annual values of the adjusted LW chronology (i.e. LWa) that can be subsequently used as a potential predictor of summer moisture independent of the EW signal (Griffin et al. 2011).

2.3 Study regions and seasonal climate response

The 15 available EW chronologies were correlated with the spring Z-index at every grid point in the US from 1895 to 1979, and the 15 LW chronologies were correlated with summer (supplemental Figs. 1–4). The 1895–1979 interval represents the common overlap between instrumental data and the tree-ring site with the earliest end date of 1979 (at Teapot Dome, WY; Table 1a). Based on the average spatial correlation patterns, we determined the sites from the northern network are best correlated with a region of the Northern Plains defined by the coordinates 43°–47°N, 107°–101°W, and the shared region of highest correlation for sites in the southern network is defined by the coordinates 35.5°–38.5°N, 105°–99°W. We calculated regional

Table 1 Sites of the EW and LW chronologies that were potential predictors for reconstruction of the regional spring and summer moisture balances

	State	Latitude	Longitude	Elevation(m)	Species	Record length	LW EPS > 0.85
A. Northern network							
1. Burning Coal Vein (BCV)	North Dakota	46.43	− 102.58	792	PIPO	1592–1990	1647
2. Eagle Nest Canyon (ENC)	South Dakota	45.21	− 103.07	1090	PIPO	1651–1991	1662
3. Reno Gulch (REN)	South Dakota	43.54	− 103.36	1740	PIPO	1370–1991	1444
4. Buckhorn Mountain (BHM)	South Dakota	43.49	− 103.31	1768	PIPO	1600–1991	1681
5. Cedar Butte (CED)	South Dakota	43.36	− 101.07	785	PIPO	1646–1991	1680
6. Teapot Dome (TEA)	Wyoming	43.23	− 106.31	1847	PIPO	1483–1979	1716
B. Southern network							
7. Black Forest East (BFE)	Colorado	39.50	− 104.22	1800	PIPO	1690–1998	1717
8. Valley View Ranch (VVF)	Colorado	39.07	− 104.43	2094	PIPO	1649–1998	1854
9. Valley View Ranch (VVR)	Colorado	39.07	− 104.43	2094	PSME	1539–1997	1623
10. Turkey Creek (TCU)	Colorado	38.21	− 104.29	1407	PIPO	1634–2003	1689
11. Kim (KIM)	Colorado	37.23	− 103.25	1650	PIPO	1698–1998	1748
12. Mesa De Maya (MDM)	Colorado	37.10	− 103.62	2060	PIPO	1631–1997	1681
13. Cornay Ranch (COR)	New Mexico	36.80	− 103.98	2020	PIPO	1613–1998	1663
14. Kenton (KEN)	New Mexico	36.49	− 103.01	1493	PIPO	1635–2015	1684
15. Sierra Grande (SIE)	New Mexico	36.43	− 103.51	2377	PIPO	1633–2014	1657

The sites were located in two sub-regions of the western Great Plains: (a) the northern network of the western Dakotas and eastern Wyoming, and (b) the southern network of eastern Colorado and northeastern New Mexico. The primary species sampled was ponderosa pine (PIPO), but there is also one site of Douglas-fir (PSME). Included is the year when the expressed population signal (EPS; Cook and Kairiukstis 1990) reaches 0.85, which is generally considered the threshold for a reliable chronology

averages of the seasonal Z-indices, and all 45 EW, LW, and LWa chronologies were then individually screened for correlation with the respective regional spring and summer moisture balances. Only EW chronologies were considered as potential predictors for the spring Z-index, and LW and LWa chronologies for the summer Z-index, in order to produce seasonal estimates that exhibited a similar correlation between spring and summer seen in the instrumental data for each region.

Based on the correlation analyses with the regionally averaged spring Z-index, we selected three EW chronologies from the Northern Plains and nine from the Southern Plains as potential predictors (bolded EW chronologies in Table 2a, b). These chronologies were selected because they contained a significant correlation with the spring Z-index, and the correlation coefficient was higher compared to summer. The same selection criterion was used for the LW and LWa chronologies for the summer Z-index (bolded LW and LWa chronologies in Table 2a, b). The LW and some of the LWa chronologies tend to be best correlated with summer moisture. However, if the correlation coefficient of the LWa chronology was not significantly different than the LW at a given site (based on Fisher's r to z transformation test), the LWa was selected as the potential predictor due to its independent variability from the EW.

Table 2 The EW, LW, and LWa chronologies from the two networks were correlated with the respective regional average spring and summer Z-indices from 1895 to 1979, and the Pearson's product moment correlation coefficients are listed

Sites	Spring Z-index		Summer Z-index		
	EW	LW	EW	LW	LWa
A. Northern Plains [43°–47°N, 107°–101°W]					
1. BCV	**0.49***	0.23*	0.36*	**0.54***	0.28*
2. ENC	**0.48***	0.51*	0.33*	0.60*	**0.51***
3. REN	0.27*	0.29*	0.28*	**0.44***	0.08
4. BHM	**0.52***	0.22*	0.38*	**0.44***	0.12
5. CED	0.33*	0.23*	0.43*	**0.55***	0.32*
6. TEA	0.41*	0.24*	0.54*	**0.30***	0.17
B. Southern Plains [35.5°–38.5°N, 105°–99°W]					
7. BFE	**0.54***	0.31*	0.42*	**0.51***	0.27*
8. VVF	**0.48***	0.40*	0.44*	0.49*	**0.33***
9. VVR	**0.55***	0.38*	0.45*	0.43*	**0.28***
10. TCU	**0.51***	0.33*	0.42*	**0.51***	0.27*
11. KIM	**0.59***	0.60*	0.34*	0.54*	**0.44***
12. MDM	**0.41***	0.32*	0.24*	**0.28***	0.15
13. COR	**0.62***	0.35*	0.41*	**0.53***	0.23*
14. KEN	**0.66***	0.33*	0.27*	0.67*	**0.56***
15. SIE	**0.52***	0.34*	0.33*	**0.40***	0.21*

Significant correlations ($p < 0.05$) are marked by *. The bolded values represent those chronologies used as the initial potential predictors of the respective seasonal climate variable. Note that if the correlation coefficient of the LWa chronology was not significantly different from the LW at a given site, the LWa was preferentially selected as a predictor

2.4 Regression modeling

Initially, all the potential predictors of the respective seasonal climate variable were submitted to a principal component regression (PCR) scheme [Cook et al. 1999; Burnette and Stahle 2010 (as recently modified by Burnette (personal communication, 2017)]. Principal component analysis (PCA; Jolliffe 2002) was computed on the selected predictor chronologies to identify modes that account for the most variance in the array. Bivariate or multivariate regression models were then used to calibrate the eigenvector amplitude time series with the instrumental Z-indices in each region over the common interval of 1945–1990. Following the initial PCR for each of the four reconstructions, we experimented with removing chronologies from the predictor pool that had the lowest correlation with the climate variable and recomputed the regression models. This was done multiple times until the most robust models were produced based on the minimum Akaike information criterion (Aikake 1974).

The reconstructed estimates were verified on independent instrumental data for the period 1900–1944. Standard regression and statistical tests were used to assess the agreement between the reconstructed estimates and instrumental data at interannual time scales, including the explained variance (adjusted R^2) in the calibration period, and the Pearson's correlation coefficient, the sign hit/miss test, the reduction of error (RE), and coefficient of efficiency (CE) in the validation period (Fritts 1976; Cook and Kairiukstis 1990; Cook et al. 1999). Spectral coherence analysis (Percival and Constantine 2006) was used to estimate how well the reconstructed estimates agree with the instrumental data at frequencies ranging from interannual to multidecadal. Early instrumental data from the nineteenth century were also used as independent validation of the spring and summer moisture balance estimates. Mock (1991) compiled nineteenth century weather data and computed seasonal precipitation percentiles for eight regions of the Great Plains, two of which were similar to the reconstructed regions in this study. The annual values from the seasonal time series plots from Mock's (1991) analysis were determined visually ("Appendix"), and then tested for correlation with the respective seasonal reconstruction during the common overlap periods. The instrumental variance lost in regression was restored to each reconstruction so that the instrumental data could be used to extend the records to 2017. However, restoration of instrumental variance can be considered a trade-off, given the error in tree-ring reconstructions tend to be amplified.

2.5 Analyses of the reconstructed data

In order to assess the ability of the seasonal tree-ring reconstructions to reproduce the largescale ocean-atmospheric teleconnections seen in the instrumental data, the instrumental and reconstructed Z-indices were correlated with the gridded SST and 500mb height fields during the calibration interval 1945–1990. Because SSTs tend to persist across months and seasons, the spring reconstructions were correlated with the December–May (DJFMAM) SSTs, and the summer reconstructions were correlated with March–August (MAMJJA). The spring (MAM) 500 mb geopotential height data were correlated with the spring reconstructions, and the same was done for summer. The significance levels of the correlations at each grid point were calculated after accounting for the potential reduced degrees of freedom due to autocorrelation in either the gridded variable or the Z-index data (Ebisuzaki 1997).

We normalized the four reconstructions (mean 0.0 and standard deviation 1.0) to compare across seasons and regions. Time series differences between the spring and summer reconstructions were calculated by subtracting the summer Z-index value from spring. A positive value indicates the Z-index value was higher for spring and vice versa. The regional difference series were then correlated with DJFMAM SST data to identify the potential teleconnections related to differences between spring and summer moisture for the full period 1856–1990. The 135 year period was chosen to provide the longest possible assessment of SST influence related to seasonal moisture differences.

Seasonal moisture reversals were defined by identifying years when the spring and summer Z-index values contained the opposite sign. The largest sign reversals were defined as years when the spring and summer Z-index values were $> \pm 0.5$ standard deviations. This was done with both instrumental and reconstructed data from 1900 to 1990 to assess how well the estimates model the largest seasonal moisture reversals. After normalization, 0.5 standard deviations equate to approximately incipient wet or dry conditions based on Palmer's (1965) scale. The time intervals between years of the same seasonal moisture reversal type (e.g. dry spring to wet summer or wet spring to dry summer) were calculated, along with their frequency distribution. The potential non-randomness of the time interval frequency distribution was then tested using the Lilliesfors test (Conover 1980; Cleaveland and Stahle 1989). Composite analysis of 500 mb height anomalies for sign changes in spring and summer moisture that exceeded $> \pm 0.25$ standard deviations in instrumental and reconstructed data were analyzed for the period 1900–1990. The lower 0.25 standard deviation threshold was used simply to increase the sample size of seasonal changes in the instrumental period. The 500 mb circulation anomalies for May represented spring, and June for summer because these months often had the most dramatic and significant changes in 500 mb heights related to seasonal moisture reversals.

3 Results

3.1 Calibration and validation statistics of the regression models

The regression models used to reconstruct the spring and summer moisture balances are presented in Table 3, and the instrumental and reconstructed time series during the calibration and validation periods along with squared coherence plots are shown in Fig. 4. The tree-ring data calibrate 39–56% of the instrumental Z-index variance and perform well against the instrumental data during the independent

Table 3 The transfer function models' calibration and validation statistics are listed for the spring (MAM) and summer (JJA) reconstructions for the (1, 2) Northern Plains and (3, 4) Southern Plains

Season	Model[a]	Chronologies used in final PCR[b]	R^2 adj.[c]	r[d]	RE/CE[e]	Sign hit/miss[f]
1. MAM	$\hat{Y}_t = -0.368 + (1.02 \times PC1_t)$	BCV* BHM* ENC*	0.39	0.65	0.39/0.39	32/13
2. JJA	$\hat{Y}_t = -0.074 + (-1.23 \times PC1_t)$	BCV$^+$ CED$^+$ ENC$^\wedge$	0.43	0.80	0.64/0.63	31/14
3. MAM	$\hat{Y}_t = -1.0645 \times PC1_t$	BFE* COR* KEN*, KIM* VVR*	0.56	0.78	0.58/0.54	34/11
4. JJA	$\hat{Y}_t = 0.034 + (-1.14 \times PC1_t)$	COR$^+$ KEN$^\wedge$ TCU$^+$	0.46	0.73	0.54/0.54	32/13

[a]The transfer function used for the reconstruction, where $\hat{Y}_t$ is the estimated Z-index value for year t and PC_t is the value for the principal component time series

[b]The final predictor chronologies used in the PCR scheme (3-letter site codes defined in Table 1), *denotes an EW chronology, $^+$LW, and $^\wedge$LWa

[c]R^2 adjusted downward for loss of degrees of freedom (Draper and Smith 1981)

[d]r = The Pearson product moment correlation coefficient between instrumental and reconstructed data in the validation period

[e]RE = reduction of error statistic (Fritts 1976); CE = coefficient of efficiency (Cook and Kairiukstis 1990)

[f]The number of occurrences in the validation period when the reconstructed data contained the same (hit) or different (miss) sign as the instrumental Z-index data

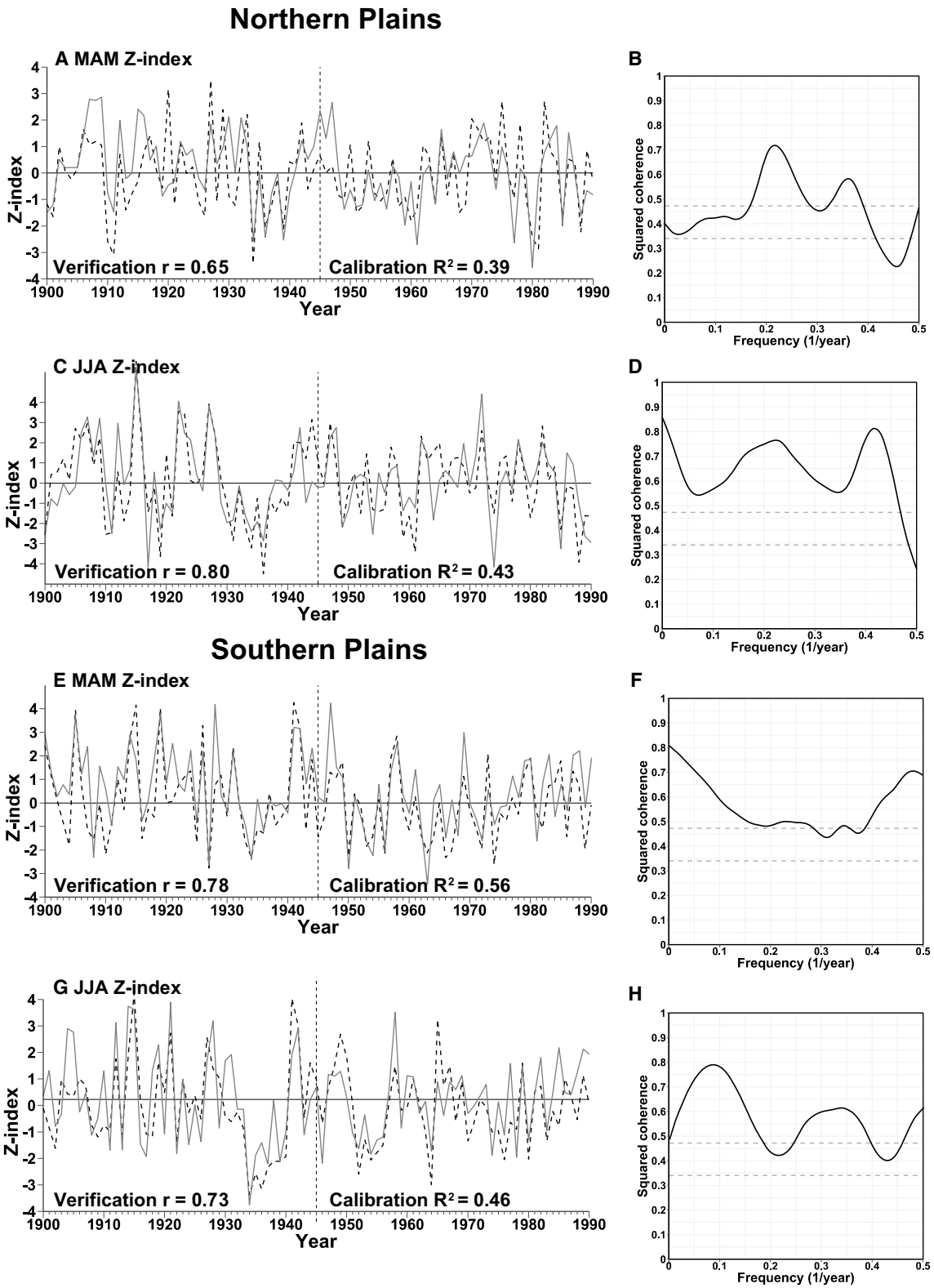

Fig. 4 The instrumental (dashed lines) and reconstructed (solid black lines) Z-indices for spring (March–May) and summer (June–August) are normalized and plotted together for the **a, c** Northern Plains and **e, g** Southern Plains from 1900 to 1990. The calibration (1945–1990) and validation (1900–1944) intervals are separated by the vertical dashed line. The statistics of each regression model are presented in Table 3. **b, d, f, h** Shown are squared coherence plots between instrumental and reconstructed Z-indices for the respective calibration and validation periods (solid black line). Dashed lines represent the 95% and 99% confidence thresholds for significant coherence

1900–1944 validation period (Table 3). Spectral coherence analysis indicates that all four reconstructions share significant common variability at $p < 0.10$ with the respective instrumental data from interannual to multidecadal frequencies (Fig. 4b, d, f, h). The results from the sign hit/miss tests indicate all reconstructions significantly ($p < 0.05$) reproduce the correct sign of the seasonal value in the validation period (Table 3). The correlations between the instrumental spring and summer moisture balances from 1900 to 1990 are $r = 0.47$ for the Northern Plains and $r = 0.33$ for the Southern Plains, similar to the reconstructed data ($r = 0.52$ and $r = 0.32$). For the full reconstruction periods, the correlation between the seasonal estimates are 0.53 from 1651 to 2017 and 0.33 from 1698 to 2017 for the northern and southern Plains, respectively.

The correlations with the independent nineteenth century weather data from Mock's (1991) seasonal precipitation data ("Appendix") also provide some additional validation of the seasonal moisture balance estimates (Table 4). The correlations with the respective seasonal moisture variable are all positive, with an r-value as high as 0.77 between spring moisture variables from the Southern Plains. The overall higher correlations for the Southern Plains may reflect the larger number of nineteenth century weather stations in this region (Mock 1991), and the stronger calibration and validation statistics achieved with the Southern Plains' reconstructions.

3.2 Ocean-atmospheric forcing of spring and summer climate in the northern and southern Plains

Correlation analyses with gridded SST data illustrate the regional and seasonal differences in large-scale SST teleconnection patterns over the northern and southern Plains (Fig. 5). The spring Z-index for the Northern Plains does not have a strong SST teleconnection signal (Fig. 5a, b), but the summer season is positively correlated with an ENSO-like pattern in the tropical Pacific and with SSTs in the Gulf of Alaska (Fig. 5c, d). The positive correlations between summer moisture in the Northern Plains and spring–summer ENSO is a finding previously reached by Bunkers et al. (1996). Mechanistically, this relationship results from ENSO's effect on the strength and positioning of the subtropical Bermuda high in the Atlantic and the summertime GPLLJ. Positive phases of ENSO during summer tend to enhance low-level moisture advection over the Great Plains due to SST and sea-level pressure gradients that develop between the tropical Pacific and subtropical Atlantic (Krishnamurthy et al. 2015). Both seasons also appear to be negatively correlated with North Atlantic SSTs, with the strongest signal present in summer (Fig. 5a–d).

Winter–spring ENSO is highly correlated with the spring Z-index for the Southern Plains (Fig. 5e, f), with correlation coefficients reaching as high as $r = 0.65$ at some grid points in the tropical Pacific based on the instrumental data. It is interesting to note that the spring moisture balances for both regions are also modestly and oppositely correlated with SSTs in the Gulf of Mexico, likely reflecting the dipole relationship with the GPLLJ. The positive (negative) correlations over the Northern Plains (Southern Plains) suggest warmer-than-normal SSTs results in a stronger GPLLJ and further northward transport of low-level moisture, generating higher precipitation totals over the Northern Plains but deficits to the south (Weaver and Nigam 2008). The summer Z-index for the Southern Plains is positively correlated with SSTs over much of the central and eastern Pacific basin, with the strongest signal present near the west coast of North America (Fig. 5g, h). Other than the Gulf of Mexico, the Atlantic teleconnections associated with spring and summer moisture over the Southern Plains are relatively weak (Fig. 5e–h).

The spatial patterns of correlation for the Northern Plains' spring Z-index and the gridded 500 mb geopotential height data resembles the negative phase of the PNA (Leathers et al. 1992), with modest negative correlations that extend across the western US (Fig. 6a, b). The typical configuration of upper-level atmospheric circulation over North America during negative phases of the PNA includes a large-scale trough centered over the northern US and southern Canada, leading to zonal flow and a more active storm track over the Northern Plains (Leathers et al. 1992). Negative phases of the PNA have also been shown to enhance the GPLLJ during the warm season months, and these combined upper-level and low-level circulation features have produced some of the wettest precipitation events on record over the north-central US (Harding and Snyder 2015). A similar pattern of negative correlations extending from the central Pacific into the western US is evident based on the correlations with the summer Z-index for the Northern Plains, along with a region

Table 4 Spring and summer precipitation percentile data for two regions similar to the reconstruction regions were obtained through visual analysis of Figs. 5 and 6 from Mock's (1991) analysis (see "Appendix")

Precipitation data	Pearson's r
Northern Plains spring Z-index (1877–1890)	0.45
Northern Plains summer Z-index (1877–1890)	0.51
Southern Plains spring Z-index (1867–1890)	0.77
Southern Plains summer Z-index (1867–1890)	0.53

Correlations analyses with the respective regional and seasonal moisture balance estimates over the common period (1877–1890 for the Northern Plains and 1867–1890 for the Southern Plains) was performed

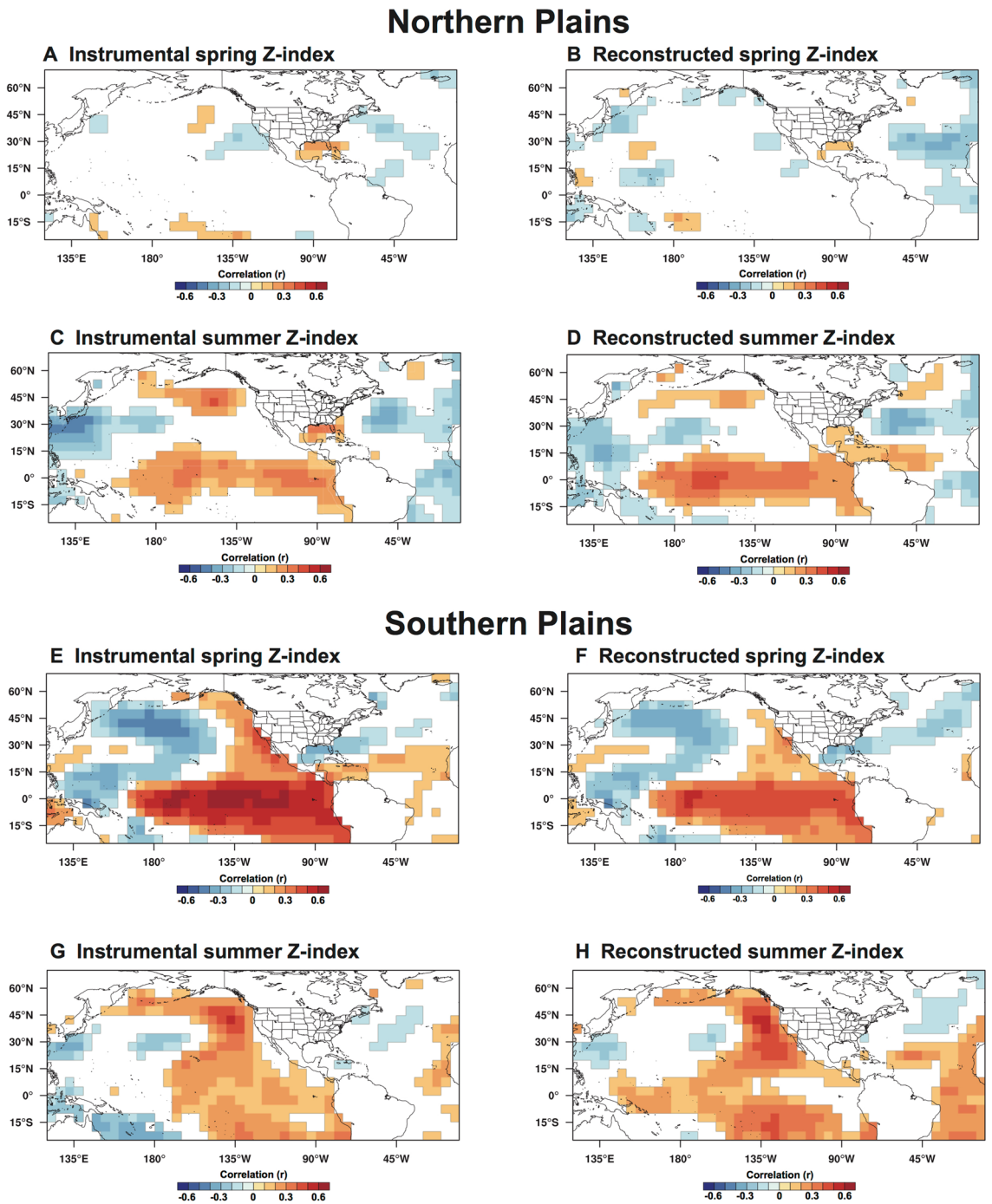

Fig. 5 The **a** instrumental and **b** reconstructed spring Z-indices for the Northern Plains reconstructed region were correlated with gridded SST data from 1945 to 1990 (Kaplan et al. 1998), after the SSTs were averaged to the winter–spring (December–May) season. The **c** Instrumental and **d** reconstructed summer Z-indices for the Northern Plains are correlated with the spring–summer (March–August) averaged SSTs. Black box represents the Northern Plains study region [43°–47°N, 107°–101°W]. **e, f** Same as **a, b** for the Southern Plains study region. **g, h** Same as **c, d** for the Southern Plains. Only grid points with significant ($p < 0.05$) correlation coefficients shown. Significance levels account for the reduced degrees of freedom due to autocorrelation in the SST and Z-index data (Ebisuzaki 1997). Black box represents the Southern Plains study region [35.5°–38.5°N, 105°–99°W]

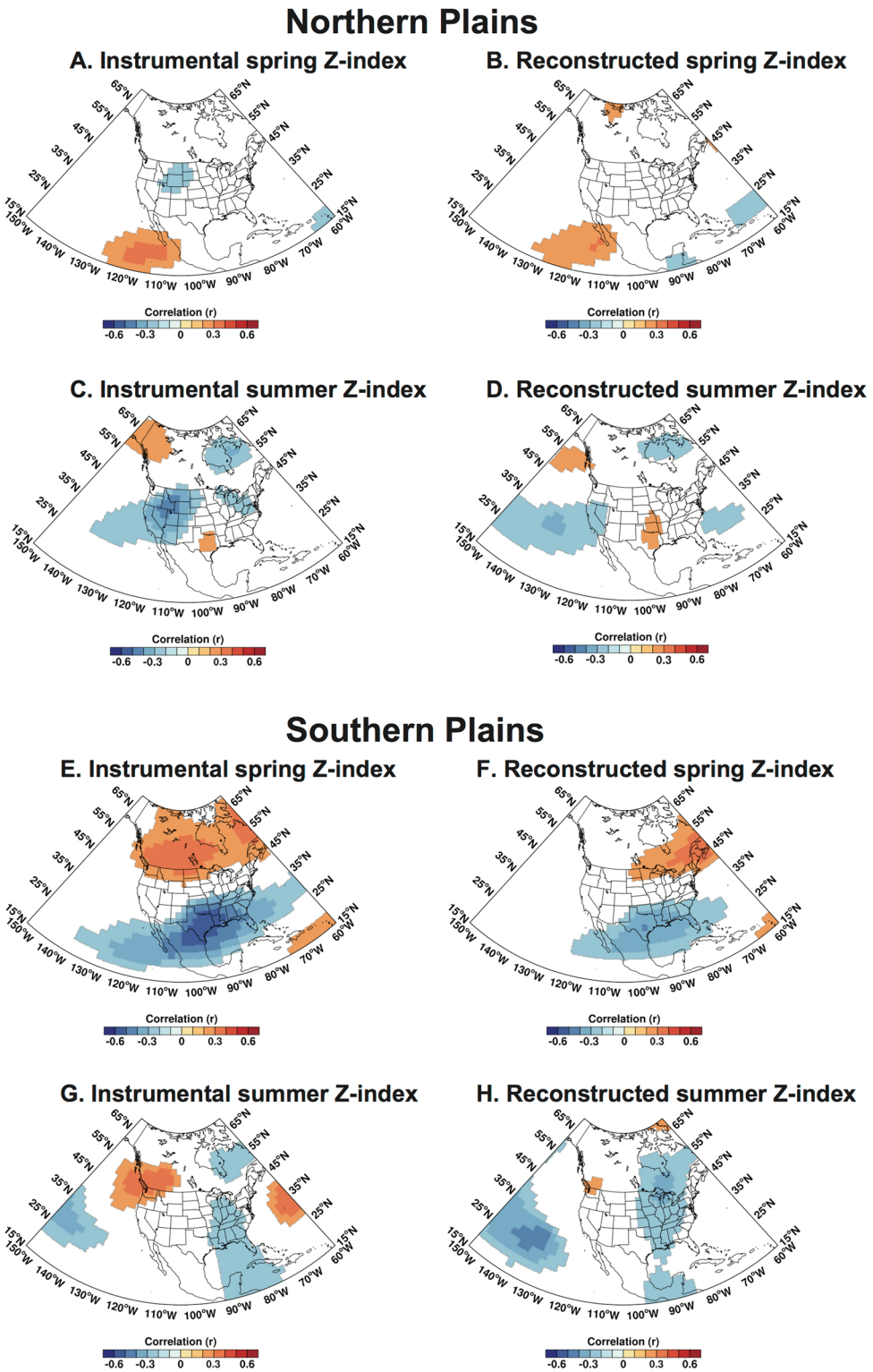

Fig. 6 The **a** instrumental and **b** reconstructed spring Z-indices for the Northern Plains reconstructed region (black box) were correlated with gridded 500mb geopotential height data from 1945 to 1990 (Kalnay et al. 1996), after the data were averaged to the spring season. The **c** Instrumental and **d** reconstructed summer Z-index for the Northern Plains were correlated with the summer averaged 500 mb geopotential height data. **e, f** Same as **a, b** for the Southern Plains study region. **g, h** Same as **c, d** for the Southern Plains. Only grid points with significant ($p < 0.05$) correlation coefficients shown. Significance levels account for the reduced degrees of freedom due to autocorrelation in the atmospheric and Z-index data

of positive correlations over the Gulf of Alaska and Southern Great Plains (Fig. 6c, d). The summertime pattern once again indicates zonal flow over the northern US and southern Canada directs more shortwave disturbances over the region, leading to wetter summers over the Northern Plains.

The spatial patterns of correlation based on the spring Z-index for the Southern Plains are consistent with the expected upper-level atmospheric circulation anomalies associated with ENSO. During positive phases of ENSO, a recurrent upper-level trough and active subtropical jet stream

resides over the southern US and northern Mexico (areas of negative correlation in Fig. 6e, f), increasing the frequency of Pacific storms and advection of subtropical moisture over the Southern Plains (Horel and Wallace 1981). The 500 mb height patterns for the summer Z-index resemble an amplified ridge-trough pattern over the US, which would result in northwest flow aloft over the study region and a greater frequency of storm systems moving southward out of Canada over the Southern Plains during the summer months (Fig. 6g, h). These SST and 500 mb correlation patterns detected in the reconstructions are remarkably to similar to the instrumental data, and indicate these seasonal estimates can reproduce the major ocean-atmospheric modes of variability associated with independent spring and summer moisture over the northern and southern Plains.

3.3 The reconstructed spring and summer moisture balances

The four reconstructions presented here offer new insight into the seasonal and spatial characteristics of major pre-instrumental era droughts, and provide a long-term seasonal context for dry conditions in the 1930s and 1950s. The normalized reconstructed spring and summer moisture balances for the two regions are plotted in Fig. 7, and the instrumental Z-indices smoothed with a 10-year cubic spline are also plotted from 1895 to 2017 to illustrate that the seasonal estimates largely track the decadal variability of the instrumental data. The reconstructions indicate that the 1930s Dust Bowl Drought represents one of the few periods when sustained summer dryness impacted both study regions. The estimated values based on the decadal splines indicate that the 1930s Dust Bowl was the worst decade of summer drought to impact the two regions concurrently in the last 300 years (Fig. 7b, d). From 1931 to 1940, the summer Z-index values are estimated to have been below normal in the northern and southern Plains seven and eight out of the 10 years, respectively. The 1930s decade also contains the highest frequency of summer drought years shared between the two regions for any 10-year period over the common 1698–2017 interval. However, spring drought during the 1930s was not as exceptional compared to summer, particularly over the Northern Plains (Fig. 7a, c). Burnette and Stahle (2013) also noted the unprecedented nature of the summer Dust Bowl Drought based on a 159-year record of July–August precipitation totals from weather stations in eastern Kansas and Missouri. Yet, when precipitation is averaged across the April–August growing season, the decadal moisture anomalies of the 1930s are not substantially more severe than other identified droughts in the nineteenth century. Similar results are evident based on the reconstructions for the northern and southern Plains and highlight the distinct seasonal nature of growing season moisture

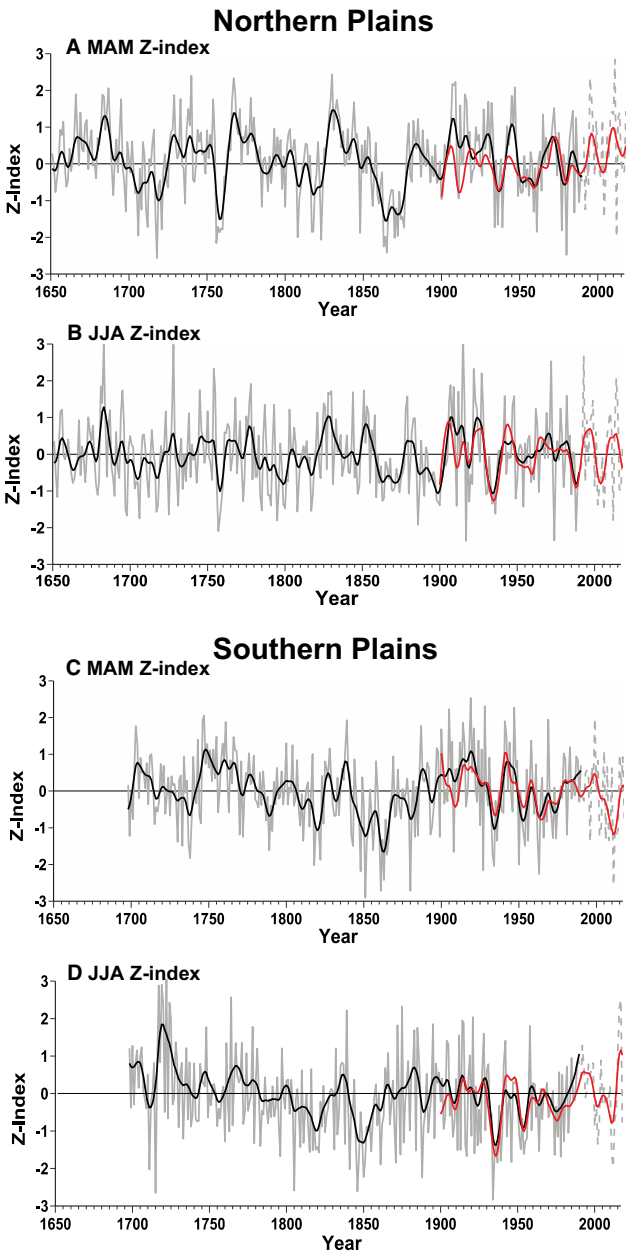

Fig. 7 The normalized **a** spring and **b** summer moisture balance reconstructions for the Northern Plains are plotted from 1651 to 1990. Reconstructions have been fit with a 10-year cubic-smoothing spline designed to emphasize decadal variability (black line; Cook and Peters 1981). **c** The spring and **d** summer moisture balance reconstructions for the Southern Plains are plotted from 1698 to 1990. Instrumental Z-index values from 1991 to 2017 are also plotted (dashed gray lines). The 10-year smoothed instrumental spring and summer Z-indices are also plotted from 1895 to 2017 (red series) with each reconstruction

conditions during the worst drought to impact the US in the modern era.

Periods when both regions in either seasons were impacted by sustained droughts do not occur frequently,

Table 5 Simple 10-year moving averages were calculated for each normalized reconstruction

Northern Plains spring	Southern Plains spring	Northern Plains summer	Southern Plains summer
1. 1860s (− 1.47)	1860s (− 1.05)	1930s (− 0.92)	1840s (− 0.98)
2. 1870s (− 0.95)	1850s (− 0.87)	1890s (− 0.70)	1930s (− 0.89)
3. 1710s (− 0.81)	1930s (− 0.61)	1860s (− 0.69)	1810s (− 0.69)
4. 1750s (− 0.72)	1810s (− 0.55)	1790s (− 0.59)	1850s (− 0.56)
5. 1950s (− 0.58)	1840s (− 0.51)	1710s (− 0.46)	1950s (− 0.46)
6. 1700s (− 0.56)	1870s (− 0.41)	1750s (− 0.38)	1970s (− 0.40)
7. 1810s (− 0.52)	1950s (− 0.33)	1780s (− 0.35)	1820s (− 0.27)
8. 1930s (− 0.45)	1960s (− 0.32)	1870s (− 0.27)	1800s (− 0.24)
9. 1890s (− 0.29)	1730s (− 0.27)	1980s (− 0.26)	1860s (− 0.16)
10. 1780s (− 0.19)	1970s (− 0.21)	1660s (− 0.22)	1780s (− 0.15)

The 10-year average for each decade (e.g. 1651–1660, 1661–1670), and the ten driest decades for each seasonal reconstruction were then identified. The 10-year average Z-index value is listed next to the decades

particularly during summer. Table 5 lists the ten driest non-overlapping decades for each season and the two regions based on a simple 10-year average. Five of the decades listed as the driest based on the spring estimates for the Northern Plains are also listed for the Southern Plains (1810s, 1860s, 1870s, 1930s, 1950s), but only three decades are shared between the summer reconstructions (1780s, 1860s, and 1930s). Worth noting, seven of the driest decades for spring are also listed for summer in both regions, suggesting a seasonal persistence in moisture balance conditions during these decadal moisture excursions.

At interannual timescales, the reconstructed spring and summer Z-indices for the Northern Plains are not correlated with the Southern Plains ($r = 0.08$ and $r = 0.11$ for spring and summer, respectively). The lack of coherence between study regions is not necessarily surprising given the different seasonal teleconnection patterns illustrated in Figs. 5 and 6. In fact, there have been several periods when seasonal conditions between the two regions exhibit opposite behavior, including in the recent twenty-first century during the spring months. Since 2003, there have been six springs with normalized values greater than 1.0 standard deviation in the Northern Plains that have co-occurred with drought conditions (< -1.0 standard deviation) to the south. The recent spring of 2011 ranks as the wettest year in the Northern Plains over the full 1651–2017 period (Fig. 7a), and this is also one of the driest springs on record for the Southern Plains (Fig. 7c). The diverging moisture balance anomalies of the early-twenty-first century between the study regions can possibly be attributed to the changing characteristics of the low-level jet and synoptic circulation over North America. Barandiaran et al. (2013) noted that a significant trend in the strength of the low-level jet has led to precipitation changes across the Great Plains in recent decades, with increases in the Northern Great Plains but decreases over the Southern Great Plains especially over Oklahoma and Texas. These changes have also coincided with a northward shift of the average springtime position of the upper-level jet stream (Wang et al. 2013), which has also contributed to these diverging spatial patterns of moisture. A 20-year running correlation between the spring Z-index data from 1698 to 2017 suggests significant periods of anti-phasing during the spring season have occurred and been greater in magnitude, but the last 20 years has been one of the most extreme ($r = -0.36$ from 1998 to 2017; not shown).

The longest sustained periods of dual-season drought to occur in either region were during the mid- and late-nineteenth century (Fig. 7). Each pair of reconstructions are plotted consecutively from 1840 to 1900 and 1930–1960, so that estimates of the spring Z-index are followed by the estimated summer Z-index for the same year to provide the most detailed comparison of spring and summer drought conditions during the nineteenth and twentieth centuries (Fig. 8). The duration and persistence of dry conditions in the mid- and late-nineteenth century do not have clear analogs in the instrumental record, especially as it relates to the spring season. Spring and summer drought estimated for the Northern Plains persisted across the two seasons beginning in the spring of 1859, and no positive Z-index value for either season is estimated until the spring of 1878 (Fig. 8a). Conditions improved in the 1880s, but spring and primarily summer drought returned in the 1890s and persisted until the beginning of the twentieth century. Drought onset occurred much earlier over the Southern Plains, approximately beginning in 1841 with few years of alleviation until 1865 (Fig. 8b).

While the 1930s Dust Bowl and 1950s drought had numerous years when above-normal or moderately dry springs preceded severe summer drought (Fig. 8c, d), drought years in the nineteenth century were often more severe during the spring season. The average seasonal Z-index values for the major nineteenth century drought intervals are substantially lower in spring for both regions

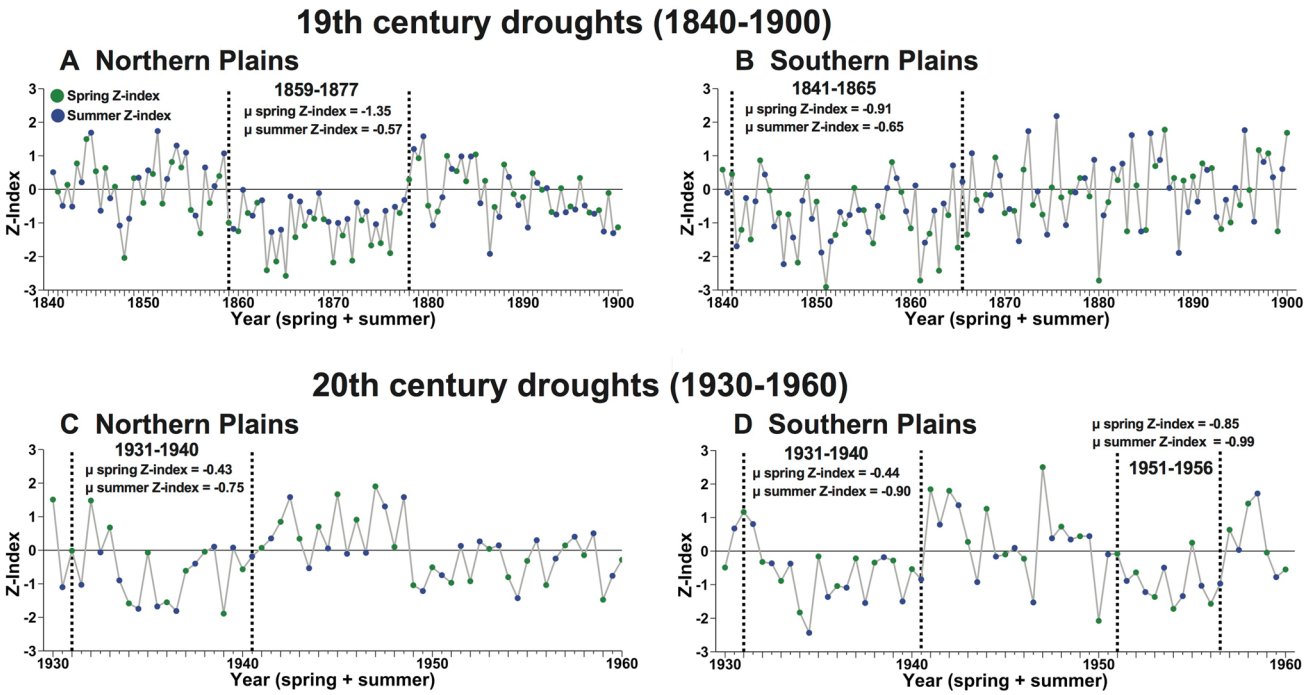

Fig. 8 **a** Reconstructed spring (green circles) and summer (blue circles) are plotted consecutively from 1840 to 1900 for the Northern Plains to highlight the distinct seasonal drought conditions of the nineteenth century. **b** Same as **a** but for the Southern Plains. **c, d** The estimates are plotted consecutively from 1930 to 1960 to illustrate the seasonality of the 1930s and 1950s Droughts for the **c** Northern Plains and **d** Southern Plains. The dashed vertical bars represent the time interval of regional drought conditions. The mean values of the two seasons for each of these intervals are also included. Note the more intense spring drought conditions in the nineteenth century, but summer drought was more severe during the 1930s and 1950s

(Fig. 8a, b), compared to the lower values in summer during the 1930s and 1950s (Fig. 8c, d). Sixteen out of the 19 estimated dual-season drought years from 1859 to 1877 were drier during the spring season over the Northern Plains (Fig. 8a), and of the 16 dual-season drought years from 1841 to 1865 estimated for the Southern Plains, ten were more severe in spring (Fig. 8b).

The few data sources from the Global Historical Climatology Network (GHCN) also seem to indicate that moisture deficits in the central US were more severe in the spring season during the droughts of the mid- to late-nineteenth century (Herweijer et al. 2006). Previous studies have documented that La Niña conditions persisted for multiple consecutive years between the 1840s and 1860s (Cole et al. 2002), providing one explanation for the more frequent and intense spring drought years over the Southern Plains from 1841 to 1865. However, the weak winter–spring ENSO signal in the Northern Plains (Fig. 5a, b) suggests drought from 1859 to 1878 was likely a separate event caused by other mechanisms, perhaps related to random atmospheric variability (Hoerling et al. 2009). Multidecadal oscillations in Atlantic and Pacific SSTs may also have influenced spring and summer drought conditions in the nineteenth century by affecting the positioning and strength of the GPLJJ (Weaver and Nigam 2008). These characteristics of seasonal drought evolution may reflect in part differences in ocean-atmospheric forcing and the influence of internal atmospheric variability, but perhaps the added anthropogenic land degradation component amplified summer drought conditions in the twentieth century (Seager et al. 2005; Cook et al. 2009).

3.4 Spring to summer moisture reversals

The reconstructions provide an extended proxy record of the frequency and temporal distribution of spring to summer moisture changes, and the potential ocean-atmospheric forcing of these seasonal differences. Of the nine largest (±0.5 standard deviations) seasonal reversals identified in the instrumental data for the Northern Plains, the reconstructions produce the correct signs of the seasonal Z-index values in five of the years. Eleven large reversal years were identified in the instrumental data for the Southern Plains, and the reconstructions reproduce the correct sign for nine of these events. Sign changes in Z-index values between spring and summer, each exceeding at least 0.5 standard deviations from the mean, are estimated to have occurred 26 times in the 367 years of the data for the Northern Plains (7%), and

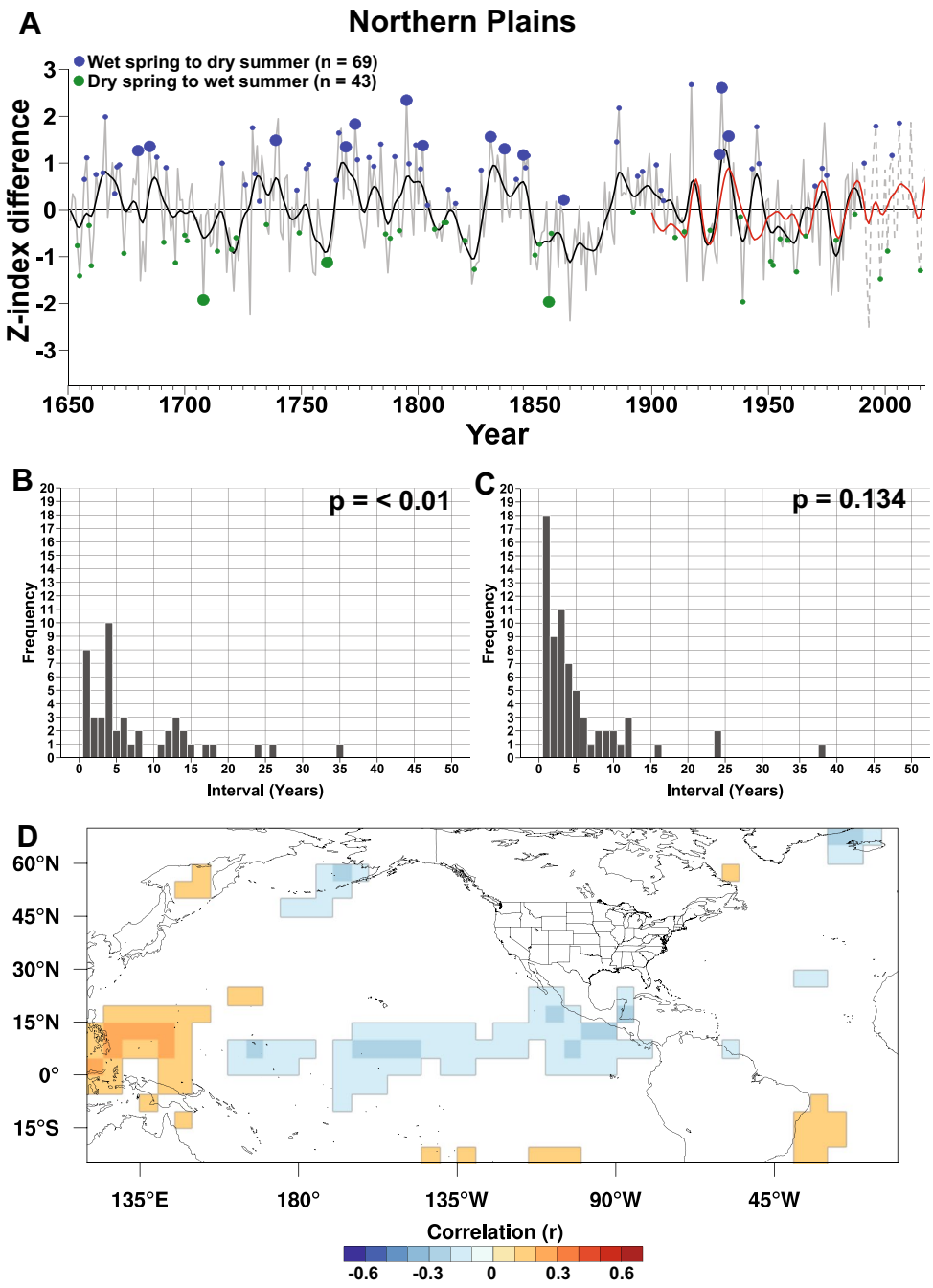

Fig. 9 **a** A time series calculated by differencing the normalized reconstructed spring Z-index from summer is plotted interannually for the Northern Plains. Values above zero are years when spring was wetter than summer, and vice versa. The time series has been fit with a 10-year spline to emphasize decadal variability (black line), and a decadal spline fit to a differenced series of the instrumental data has also been included (red line). The blue and green points represent a change in sign of the moisture balance from spring to summer, with blue points indicating a wet spring followed by a dry summer, and green points are the opposite pattern. Large blue and green dots represent seasonal moisture reversals when both the spring and summer Z-index values were 0.5 standard deviations above or below the mean. **b** The histogram of return intervals for dry springs followed by wet summers (p values test the distribution of return intervals for non-randomness; $p < 0.05$ = non-random distribution). **c** Same as **b** for wet springs followed by dry summers. **d** The reconstructed differenced series was correlated with December–May (DJFMAM) SST data from 1856 to 1990. Only grid points with significant ($p < 0.05$) correlation coefficients are plotted

28 out of 320 years (9%) in the Southern Plains (larger blue and green dots in Figs. 9a, 10a).

The differenced series shown in Figs. 9a and 10a illustrate the decadal to multidecadal variability in the relationship between the two seasons and in the occurrence of the largest moisture reversals. Decadal estimates of the reconstructed differenced series are significantly correlated with the instrumental data ($r = 0.57$ and 0.65 for the northern and southern Plains, respectively). For much of the nineteenth century, summer conditions are estimated to have been more favorable in summer over the Northern Plains, exemplified by the large differences in moisture balance values during the 1820s and from the late-1840s to early-1880s. In the recent decades spring values on average have been higher compared to summer based on the decadal spline, but there has been substantial interannual variability between the two seasons. The differenced estimates for the Southern Plains indicate that for much of the early-eighteenth century conditions were wetter in summer with a greater probability for drier springs to precede

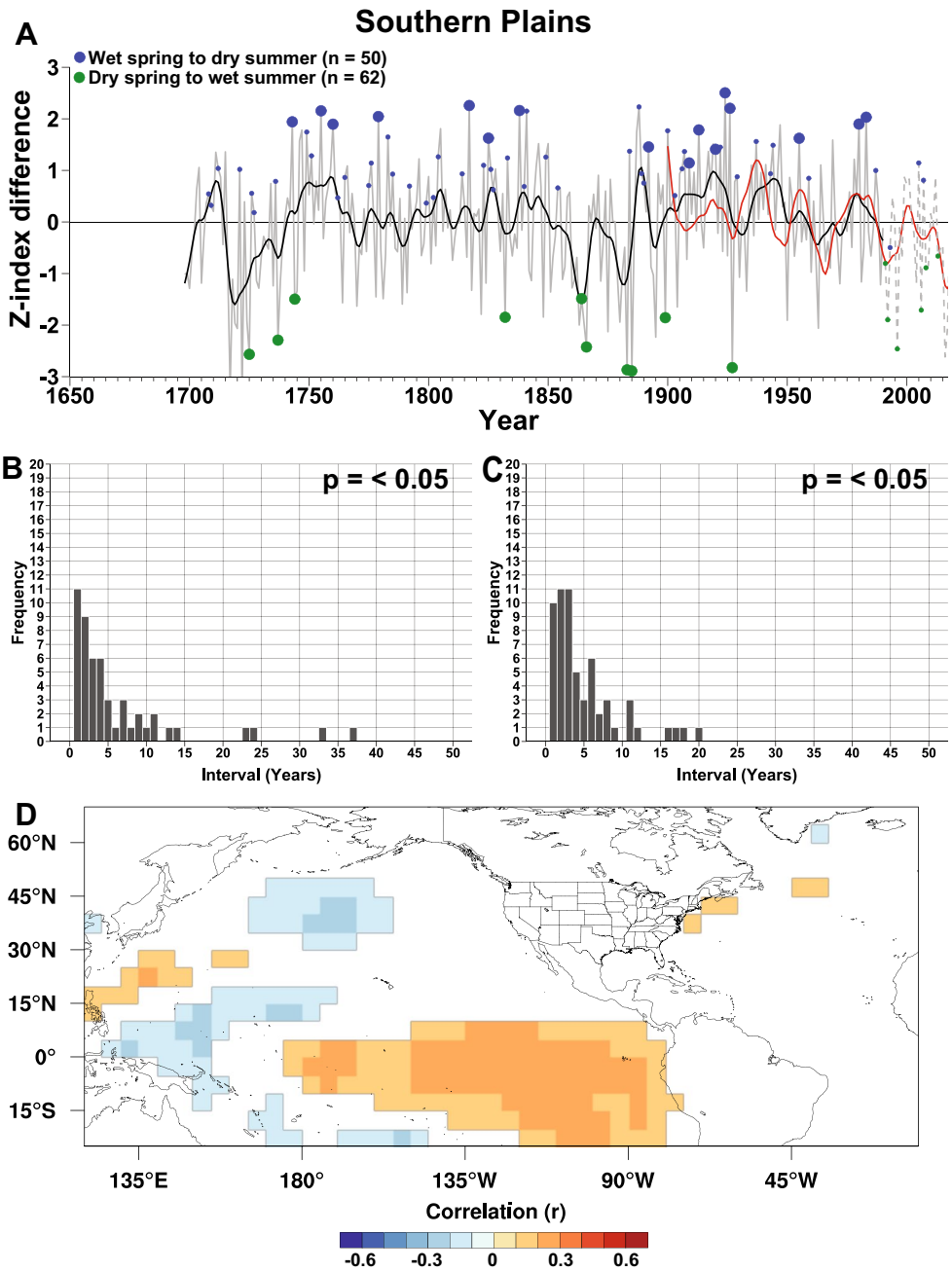

Fig. 10 Same as Fig. 10 for the Southern Plains

wet summers. Conditions appear to have reversed in the late-18th and early-nineteenth centuries, when springs are estimated to have been wetter. Likewise, in the late-twentieth century wetter springs punctuated an overall favorable spring and summer growing season, but in the recent two decades springs have become drier over the Southern Plains.

The time intervals between seasonal moisture reversal years seem to exhibit nonrandom behavior. The distributions of return intervals fail to reject the null hypothesis of randomness based on the Lilliefors test for three of the reconstructions ($p < 0.05$; Figs. 10b, 11b, c), the exception being spring drought alleviation events estimated for the Northern Plains (Fig. 10c). Seasonal moisture reversals most often occur the 1–5 years following a reversal of the same sign. However, there are estimated to have been multidecade periods between moisture reversals, the longest being 37 years from 1857 to 1893 for dry springs to wet summers in the Northern Plains. The non-randomness identified in the return intervals of reconstructed moisture reversals is also evident in the instrumental data (not shown).

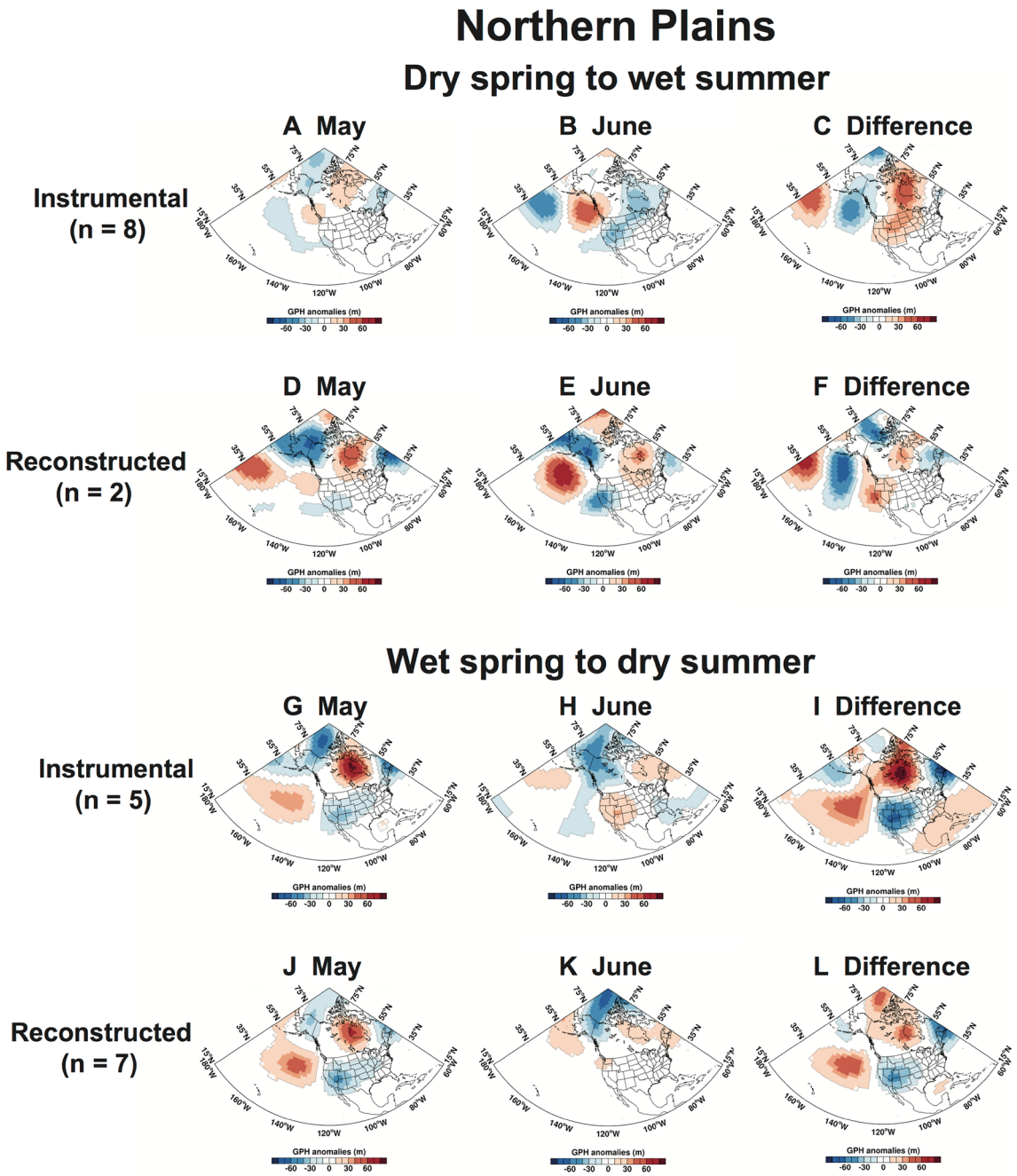

Fig. 11 **a, d** Dry springs to **b, e** wet summers and **g, j** wet springs to **h, k** dry summers that exceeded > ±0.25 standard deviations were identified in instrumental and reconstructed data from 1900 to 1990 for the Northern Plains. The 500 mb height anomalies for May vs. June were composited for the identified reversal years in instrumental and reconstructed data. **c, f, i, l** Differences in 500 mb height from May to June (May–June) are plotted. Shaded regions in the composite maps of May and June indicate significant ($p < 0.05$) anomalies relative to the monthly climatology calculated from 1981 to 2010

The spring to summer moisture reversals may be related in part to large-scale ocean-atmospheric teleconnection patterns. Correlation analyses between the differenced series for the Northern Plains and SST data from 1856 to 1990 indicate a modest relationship with La Niña conditions in the Pacific. This weak La Niña signal can be explained in part by the differences in the ENSO teleconnection from spring to summer (Fig. 5a–d). Winter–spring La Niña conditions would increase the likelihood of a drier summer over the Northern Plains but would not have a significant impact on the spring climate, thus leading to a higher probability for a larger spring Z-index value. The spatial correlation patterns

associated with seasonal differences in the Southern Plains indicate a pattern representative of the positive phase of ENSO in the Pacific (Fig. 10d). El Niño conditions during the winter and spring seasons would favor a wet spring over the Southern Plains, and as a result, an increased likelihood that the spring Z-index value would be higher compared to the summer. These SST correlation patterns appear to be stable through time based on non-overlapping 45 year correlation periods, though the strongest signals are present in the most recent 45 years (not shown).

Major seasonal moisture reversals sometimes reflect significant changes in mid-tropospheric flow over the Pacific-North American sector from spring to summer, especially for the last month of spring and the first month of summer (i.e. May vs. June). Shown in Fig. 11 are composites of the 500 mb height anomalies for seasonal moisture reversals exceeding 0.25 standard deviations identified in the instrumental and reconstructed data for the Northern Plains (the anomalies for the Southern Plains are weak and not shown). The largest differences in atmospheric circulation from May to June are observed in both instrumental and reconstructed data over the western US for wet springs that precede dry summers (Fig. 11g–l). Positive height anomalies over the Gulf of Alaska and a downstream trough in May (Fig. 11g, j) are replaced with nearly the opposite circulation patterns in June (Fig. 11h, k, l). Wet summers that follow drier springs appear to be connected to slightly-above or near-normal 500 mb heights over the western US in May (Fig. 11a, d), but the anomaly patterns for June indicate a shift to zonal flow (Fig. 11b, e). Despite the low 0.25 standard deviation threshold, these moisture reversals are relatively rare events, and their occurrence and distribution over time does not appear to be random. This suggests that atmospheric mechanisms related to major moisture reversals may be influenced by other low-frequency modes of variability that create large-scale environments conducive for significant and sometimes sudden seasonal changes in upper-level circulation over North America.

Analyses of major reversals over the Southern Plains do not indicate any large changes in atmospheric circulation from May to June, or spring to summer over the US. However, one of the largest spring to summer moisture reversals over the Southern Plains in both the instrumental and reconstructed series is 1980 (Fig. 10a). This unusual year was associated with a rapid change in atmospheric circulation as discussed by Namias (1982). A deep trough over the southwestern US during May was replaced within a week in late-May and early-June by a persistent omega-type blocking ridge over the Southern Plains. These observations indicate that some of the strongest spring to summer moisture reversals in the Southern Plains do reflect substantial changes in seasonal atmospheric circulation anomalies, and previous events of this magnitude in the reconstructed record may reflect similar conditions.

4 Conclusions

Separate seasonal moisture signals are encoded in EW, LW, and LWa width chronologies from the northern and southern Plains. Reconstructions of the seasonal atmospheric moisture balance (Palmer's Z-index) have been developed for both regions, although the reconstruction for the spring season in the Northern Plains study area only represents 39% of the variance in the instrumental record. Estimates of the spring Z-index for the Northern Plains may be improved with additional sampling of sites and species where the potential EW growth is in response primarily to spring moisture. Field sampling strategies tailored towards producing LW and LWa chronologies (e.g. Griffin et al. 2011) could also improve estimates of summer moisture. Nonetheless, select historical observations of weather and climate from the nineteenth century add independent support for some of the seasonal reconstructions, as do the similar SST and 500 mb geopotential height anomaly patterns linked with instrumental spring and summer moisture variability during the twentieth century.

The derived reconstructions document the seasonal climate history of the northern and southern Plains and highlight the intra-annual to multidecadal variability of regional spring and summer moisture. The 1930s Dust Bowl drought may have been the most extreme summer drought to impact the northern and southern Plains in the last few centuries, but drought conditions in spring were not substantially more severe compared to other periods. Our results suggest that the 1930s may have been the only decadal episode of summer drought to simultaneously impact both the study areas since the late-seventeenth century. Comparatively, sustained dual-season drought characterized the mid- and late-nineteenth century, and it appears the driest conditions most often occurred during the spring months. The differences in seasonality associated with these major instrumental and historical-era droughts, and the large-scale ocean-atmospheric dynamics responsible for these estimated seasonal differences, is an important research topic requiring further investigation. The seasonal reconstructions also suggest that the spring and summer climates of the northern and southern Plains are largely independent, and in recent decades there has been significant divergence in spring moisture trends possibly attributable to changes in low-level moisture advection from the GPLLJ and position of the upper-level westerly jet stream.

The seasonal reconstructions provide an extended proxy record of the infrequent spring to summer moisture reversals. These seasonal moisture changes in the Northern Plains

appear to be related in part to SST anomalies in the Pacific and to changes in mid-tropospheric circulation from spring to summer over the North Pacific and western North America. Separate reconstructions of spring and summer moisture conditions from tree-ring chronologies of EW, LW, and LWa width more broadly across the US will improve our understanding of the history of seasonal climate variability and provide insight into the large-scale ocean-atmospheric mechanisms responsible for these seasonal regimes.

Acknowledgements We thank Connie Woodhouse and David Meko for use of their tree-ring collections from the Great Plains, and Chris Baisan, Peter Brown, Cary Mock, and Dorian Burnette for advice and assistance. This study was funded by the National Science Foundation (Grant #AGS-1266014).

Appendix

Year	NP spring percentiles	NP summer percentiles	SP spring percentiles	SP summer percentiles
1867	NA	NA	100	55
1868	NA	NA	45	170
1869	NA	NA	150	90
1870	NA	NA	70	100
1871	NA	NA	70	50
1872	NA	NA	210	215
1873	NA	NA	120	105
1874	NA	NA	130	45
1875	NA	NA	80	175
1876	NA	NA	75	110
1877	145	40	130	90
1878	155	90	140	125
1879	180	190	75	100
1880	140	170	40	180
1881	100	80	85	110
1882	105	120	140	80
1883	65	75	80	75
1884	75	150	150	110
1885	110	105	100	160
1886	90	45	110	120
1887	85	150	160	100
1888	115	125	130	110
1889	70	65	100	70
1890	125	45	100	80

Precipitation percentiles from Mock's (1991) analysis of nineteenth century weather for the two regions that are closest to the Northern Plains (NP) and Southern Plains (SP) study area

References

Akaike H (1974) A new look at statistical model identification. IEEE Trans Autom Control 19:716–723. https://doi.org/10.1109/TAC.1974.1100705

Barandiaran D, Wang SY, Hilburn K (2013) Observed trends in the Great Plains low-level jet and associated precipitation changes in relation to recent droughts. Geophys Res Lett 40:6247–6251. https://doi.org/10.1002/2013GL058296

Bunkers MJ, Miller JR, DeGaetano AT (1996) An examination of El Niño-La Niña-related precipitation and temperature anomalies across the northern plains. J Clim 9:147–160. https://doi.org/10.1175/1520-0442(1996)009%3C0147:AEOENN%3E2.0.CO;2

Burnette DJ, Stahle DW (2010) Program DendroTools. Tree Ring Lab, University of Arkansas, Fayetteville

Burnette DJ, Stahle DW (2013) Historical perspective on the dust bowl drought in the central United States. Clim Change 116:479–494. https://doi.org/10.1007/s10584-012-0525-2

Burns JN, Acuna-Soto R, Stahle DW (2014) Drought and epidemic typhus, central Mexico, 1655–1918. Emerg Infect Dis 20:442–447. https://doi.org/10.3201/eid2003.131366

Cleaveland MK, Duvick DN (1992) Iowa climate reconstructed from tree rings, 1640–1982. Water Resour Res 28:2607–2615. https://doi.org/10.1029/92WR01562

Cleaveland MK, Stahle DW (1989) Tree ring analysis of surplus and deficit runoff in the White River, Arkansas. Water Resour Res 25:1391–1401. https://doi.org/10.1029/WR025i006p01391

Cleaveland MK, Stahle DW, Therrell MD et al (2003) Tree-ring reconstructed winter precipitation and tropical teleconnections in Durango. Mexico Clim Change 59:369–388. https://doi.org/10.1023/A:1024835630188

Cole JE, Overpeck JT, Cook ER (2002) Multiyear La Nina events and persistent drought in the contiguous United States. Geophys Res Lett. https://doi.org/10.1029/2001GL013561

Compo GP, Whitaker JS, Sardeshmukh PD et al (2011) The twentieth century reanalysis project. Q J R Meteorol Soc 137:1–28

Conover W (1980) Practical nonparametric statistics. Wiley, New York

Cook ER (1985) A time series analysis approach to tree ring standardization. Dissertation, University of Arizona, p 171

Cook ER, Kairiukstis LA (1990) Methods of dendrochronology. Kluwer Academic Publishers, Boston

Cook ER, Peters K (1981) The smoothing spline: a new approach to standardizing forest interior tree-ring width series for dendroclimatic studies. Tree-Ring Bull 41:45–53

Cook ER, Meko DM, Stahle DW, Cleaveland MK (1999) Drought reconstructions for the continental United States. J Clim 12:1145–1163. https://doi.org/10.1175/1520-0442

Cook ER, Seager R, Cane MA, Stahle DW (2007) North American drought: reconstructions, causes, and consequences. Earth Sci Rev 81:93–134. https://doi.org/10.1016/j.earscirev.2006.12.002

Cook BI, Miller RL, Seager R (2009) Amplification of the North American "Dust Bowl" drought through human-induced land degradation. Proc Natl Acad Sci 106:4997–5001. https://doi.org/10.1073/pnas.0810200106

Cook ER, Krusic PJ, Melvin TM (2014) Program RCSigFree. Tree ring Lab, Lamont Doherty Earth Observatory of Columbia University, Palisades

Crawford CJ, Griffin D, Kipfmueller KF (2015) Capturing season-specific precipitation signals in the northern Rocky Mountains, USA, using earlywood and latewood tree rings. J Geophys Res Biogeosci 120:428–440. https://doi.org/10.1002/2014JG002740

Dai A (2001) Global precipitation and thunderstorm frequencies. Part II: Diurnal variations. J Clim 14:1112–1128. https://doi.org/10.1175/1520-0442

Daly C, Neilson RP, Phillips DL (1994) A statistical-topographic model for mapping climatological precipitation over mountainous terrain. J Appl Meteorol 33:140–158. https://doi.org/10.1175/1520-0450

Dannenberg MP, Wise EK (2016) Seasonal climate signals from multiple tree ring metrics: a case study of *Pinus ponderosa* in the upper Columbia River Basin. J Geophys Res Biogeosci 121:1178–1189. https://doi.org/10.1002/2015JG003155

Donat MG, King AD, Overpeck JT et al (2016) Extraordinary heat during the 1930s US Dust Bowl and associated large-scale conditions. Clim Dyn 46:413–426. https://doi.org/10.1007/s00382-015-2590-5

Draper NR, Smith H (1981) Applied regression analysis. Wiley, New York

Ebisuzaki W (1997) A method to estimate the statistical significance of a correlation when the data are serially correlated. J Clim 10:2147–2153. https://doi.org/10.1175/1520-0442(1997)010%3C2147:AMTETS%3E2.0.CO;2

Enfield DB, Mestas-Nuñez AM, Trimble PJ (2001) The Atlantic multidecadal oscillation and its relation to rainfall and river flows in the continental US. Geophys Res Lett 28:2077–2080. https://doi.org/10.1029/2000GL012745

Faulstich HL, Woodhouse CA, Griffin D (2013) Reconstructed cool- and warm-season precipitation over the tribal lands of northeastern Arizona. Clim Change 118:457–468. https://doi.org/10.1007/s10584-012-0626-y

Feng S, Trnka M, Hayes M, Zhang Y (2017) Why do different drought indices show distinct future drought risk outcomes in the US Great Plains? J Clim 30:265–278. https://doi.org/10.1175/JCLI-D-15-0590.1

Fritsch JM, Kane RJ, Chelius CR (1986) The contribution of mesoscale convective weather systems to the warm-season precipitation in the United States. J Clim Appl Meteorol 25:1333–1345

Fritts HC (1965) Tree ring evidences for climatic changes in western North America. Mon Weather Rev 93:421–443

Fritts HC (1976) Tree rings and climate. Blackburn Press, Clarendan

Griffin D, Meko DM, Touchan R et al (2011) Latewood chronology development for summer-moisture reconstruction in the US southwest. Tree Ring Res 67:87–101. https://doi.org/10.3959/2011-4.1

Griffin D, Woodhouse CA, Meko DM et al (2013) North American monsoon precipitation reconstructed from tree-ring latewood. Geophys Res Lett 40:954–958. https://doi.org/10.1002/grl.50184

Harding KJ, Snyder PK (2015) The relationship between the Pacific-North American teleconnection pattern, the Great Plains low-level jet, and north central US heavy rainfall events. J Clim 28:6729–6742. https://doi.org/10.1175/JCLI-D-14-00657.1

Herweijer C, Seager R, Cook ER (2006) North American droughts of the mid to late nineteenth century: a history, simulation and implication for Mediaeval drought. Holocene 16:159–171. https://doi.org/10.1191/0959683606hl917rp

Higgins RW, Yao Y, Yarosh ES, et al (1997) Influence of the Great Plains low-level jet on summertime precipitation and moisture transport over the central United States. J Clim 10:481–507. https://doi.org/10.1175/1520-0442(1997)010%3C0481:IOTGPL%3E2.0.CO;2

Hirschboeck K (1991) Climate and floods: national water summary, 1988–1989—floods and droughts: hydrologic perspective on water issues. US Geological Survey Water-Supply Paper 2375, pp 67–88

Hoaglin DC, Mosteller F, Tukey JW (2000) Understanding robust and exploratory data analysis. Wiley, New York

Hoerling M, Quan XW, Eischeidi J (2009) Distinct causes for two principal US droughts of the 20th century. Geophys Res Lett. https://doi.org/10.1029/2009GL039860

Hoerling M, Kumar A, Dole R, Nielsen-Gammon JW, Eischeid J, Perlwitz J, Quan XW, Zhang T, Pegion P, Chen M (2013) Anatomy of an extreme event. J Clim 26(9):2811–2832

Hoerling M, Eischeid J, Kumar A et al (2014) Causes and predictability of the 2012 Great Plains drought. Bull Am Meteorol Soc 95:269–282. https://doi.org/10.1175/BAMS-D-13-00055.1

Horel JD, Wallace JM (1981) Planetary-scale phenomena associated with the Southern Oscillation. Mon Weather Rev 109:813–829. https://doi.org/10.1175/1520-0493(1981)109%3C0813:PSAPAW%3E2.0.CO;2

Hu Q, Feng S (2010) Influence of the Arctic oscillation on central United States summer rainfall. J Geophys Res 115:13. https://doi.org/10.1029/2009jd011805

Jolliffe IT (2002) Principal component analysis, 2nd edn. Springer, New York

Kalnay E, Kanamitsu M, Kistler R et al (1996) The NCEP/NCAR 40-year reanalysis project. Bull Am Meteorol Soc 77:437–471. https://doi.org/10.1175/1520-0477

Kaplan A, Cane MA, Kushnir Y et al (1998) Analyses of global sea surface temperature 1856–1991. J Geophys Res 103589:567–618. https://doi.org/10.1029/97JC01736

Karl TR (1986) The sensitivity of the palmer drought severity index and palmer's Z-index to their calibration coefficients including potential evapotranspiration. J Clim Appl Meteorol 25:77–86. https://doi.org/10.1175/1520-0450

Karl TR, Quayle RG, Karl TR, Quayle RG (1981) The 1980 summer heat wave and drought in historical perspective. Mon Weather Rev 109:2055–2073. https://doi.org/10.1175/1520-0493

Karl T, Quinlan F, Ezell DS (1987) Drought termination and amelioration: its climatological probability. J Clim Appl Meteorol 26:1198–1209

Krishnamurthy L, Vecchi GA, Msadek R et al (2015) The seasonality of the Great Plains low-level Jet and ENSO relationship. J Clim 28:4525–4544. https://doi.org/10.1175/JCLI-D-14-00590.1

Leathers DJ, Palecki MA (1992) The Pacific North-American teleconnection pattern and United-States climate. 29 temporal characteristics and index specification. J Clim 5:707–716. https://doi.org/10.1175/1520-0442(1992)005%3C0707:Tpatpa%3E2.0.Co;2

Little EL (1971) Atlas of the United States trees, Volume 1, Conifers and important hardwoods. US Department of Agriculture Miscellaneous publications

Mantua NJ, Hare SR (2002) The Pacific decadal oscillation. J Oceanogr 58:35–44. https://doi.org/10.1023/A:1015820616384

Meko DM, Baisan CH (2001) Pilot study of latewood-width of conifers as an indicator of variability of summer rainfall in the North American monsoonregion. Int J Climatol 21:697–708. https://doi.org/10.1002/joc.646

Melvin TM, Briffa KR (2008) A "signal-free" approach to dendroclimatic standardisation. Dendrochronologia 26:71–86. https://doi.org/10.1016/j.dendro.2007.12.001

Mo KC, Lettenmaier DP (2016) Precipitation deficit flash droughts over the United States. J Hydrometeorol 17:1169–1184. https://doi.org/10.1175/JHM-D-15-0158.1

Mock CJ (1991) Drought and precipitation fluctuations in the Great Plains during the late nineteenth century. Gt Plains Res 1:26–57

Mock CJ (1996) Climatic controls and spatial variations of precipitation in the western United States. J Clim 9:1111–1124. https://doi.org/10.1175/1520-0442

Muhs DR, Holliday VT (1995) Evidence of active dune sand on the Great Plains in the 19th century from accounts of early explorers. Quat Res 43:198–208. https://doi.org/10.1006/qres.1995.1020

Namias J (1982) Anatomy of Great Plains protracted heat waves (especially the 1980 US summer drought). Mon Weather Rev 110:824–838. https://doi.org/10.1175/1520-0493

Palmer WC (1965) Meteorological Drought. US Weather Bureau. Res Pap No 45, 58

Percival DB, Constantine WLB (2006) Exact simulation of Gaussian time series from nonparametric spectral estimates with application to bootstrapping. Stat Comput 16:25–35. https://doi.org/10.1007/s11222-006-5198-0

Ropelewski CF, Halpert MS (1987) Global and regional scale precipitation patterns associated with the El Niño/Southern Oscillation. Mon Weather Rev 115:1606–1626. https://doi.org/10.1175/1520-0493(1987)115%3C1606:GARSPP%3E2.0.CO;2

Ruiz-Barradas A, Nigam S (2005) Warm season rainfall variability over the US Great Plains in observations, NCEP and ERA-40 reanalyses, and NCAR and NASA atmospheric model simulations. J Clim 18:1808–1830. https://doi.org/10.1175/JCLI3343.1

Sauchyn DJ, Skinner WR (2001) A proxy record of drought severity for the Southwestern Canadian Plains. Can Water Resour J 26:253–272

Schulman E (1942) Dendrochronology in pines of Arkansas. Ecology 23:309–318

Seager R, Kushnir Y, Herweijer C et al (2005) Modeling of tropical forcing of persistent droughts and pluvials over western North America: 1856–2000. J Clim 18:4065–4088. https://doi.org/10.1175/JCLI3522.1

Sieg CH, Meko D, Ni W (1996) Dendroclimatic potential in the northern Great Plains. In: Dean JS, Meko DM, Swetnam TW (eds) Tree rings, environment and humanity. Radiocarbon (International radiocarbon conference). University of Arizona, Tucson, pp 295–302

St. George S, Meko DM, Girardin MP et al (2009) The tree-ring record of drought on the Canadian Prairies. J Clim 22:689–710. https://doi.org/10.1175/2008JCLI2441.1

Stahle DW, Cleaveland MK (1988) Texas drought history reconstructed and analyzed from 1698 to 1980. J Clim 1:59–74

Stahle DW, Cleaveland MK, Grissino-Mayer HD et al (2009) Cool- and warm-season precipitation reconstructions over western New Mexico. J Clim 22:3729–3750. https://doi.org/10.1175/2008JCLI2752.1

Stockton D, Meko D (1983) Drought recurrence in the Great Plains as reconstructed from long-term tree ring records. J Clim Appl Meteorol 22:17–29

Stokes MA, Smiley TL (1996) An introduction to tree-ring dating. University of Arizona Press, Tucson, AZ

Therrell MD, Stahle DW, Cleaveland MK, Villanueva-Diaz J (2002) Warm season tree growth and precipitation over Mexico. J Geophys Res Atmos. https://doi.org/10.1029/2001JD000851

Torbenson MCA, Stahle DW (2018) The relationship between cool and warm season moisture over the central United States, 1685–2015. J Clim. https://doi.org/10.1175/JCLI-D-17-0593.1

Villanueva-Diaz J, Stahle DW, Luckman BH et al (2007) Winter–spring precipitation reconstructions from tree rings for northeast Mexico. Clim Change 83:117–131. https://doi.org/10.1007/s10584-006-9144-0

Wang SY, Chen TC (2009) The late-spring maximum of rainfall over the US central plains and the role of the low-level jet. J Clim 22:4696–4709. https://doi.org/10.1175/2009JCLI2719.1

Wang SY, Davies RE, Gillies RR (2013) Identification of extreme precipitation threat across midlatitude regions based on short-wave circulations. J Geophys Res Atmos 118:11059–11074. https://doi.org/10.1002/jgrd.50841

Watson E, Luckman BH (2002) The dendroclimatic signal in Douglas-fir and ponderosa pine tree-ring chronologies from the southern Canadian Cordillera. Can J For Res 32:1858–1874. https://doi.org/10.1139/x02-096

Watson E, Luckman BH (2004) Tree-ring based reconstructions of precipitation for the southern Canadian Cordillera. Clim Change 65:209–241. https://doi.org/10.1023/B:CLIM.0000037487.83308.02

Weaver SJ, Nigam S (2008) Variability of the Great Plains low-level jet: large-scale circulation context and hydroclimate impacts. J Clim 21:1532–1551. https://doi.org/10.1175/2007JCLI1586.1

Weaver SJ, Nigam S (2011) Recurrent supersynoptic evolution of the Great Plains low-level Jet. J Clim 24:575–582. https://doi.org/10.1175/2010JCLI3445.1

Wells PV, Kilham L, Moloney JB (1965) Scarp woodlands, transported grassland soils, and concept of grassland climate in the Great Plains Region. Science 148:246–249. https://doi.org/10.1126/science.148.3667.246

Woodhouse C, Brown PM (2001) Tree-ring evidence for Great Plains drought. Tree Ring Res 57:89–103

Woodhouse CA, Overpeck JT (1998) 2000 years of drought variability in the central United States. Bull Am Meteorol Soc 79:2693–2714. https://doi.org/10.1175/1520-0477

Woodhouse CA, Meko DM, Griffin D, Castro CL (2013) Tree rings and multiseason drought variability in the lower Rio Grande Basin, USA. Water Resour Res 49:844–850. https://doi.org/10.1002/wrcr.20098